Solution of the Riemann problem for polarization waves in a two-component Bose-Einstein condensate

S. K. Ivanov,[1,2] A. M. Kamchatnov,[1,2] T. Congy,[3] and N. Pavloff[3]

[1]*Institute of Spectroscopy, Russian Academy of Sciences, Troitsk, Moscow 108840, Russia*
[2]*Moscow Institute of Physics and Technology, Institutsky lane 9, Dolgoprudny, Moscow region 141700, Russia*
[3]*LPTMS, CNRS, Univ. Paris-Sud, Université Paris-Saclay, 91405 Orsay, France*

We provide a classification of the possible flows of two-component Bose-Einstein condensates evolving from initially discontinuous profiles. We consider the situation where the dynamics can be reduced to the consideration of a single polarization mode (also denoted as "magnetic excitation") obeying a system of equations equivalent to the Landau-Lifshitz equation for an easy-plane ferromagnet. We present the full set of one-phase periodic solutions. The corresponding Whitham modulation equations are obtained together with formulas connecting their solutions with the Riemann invariants of the modulation equations. The problem is not genuinely nonlinear, and this results in a non-single-valued mapping of the solutions of the Whitham equations with physical wave patterns as well as the appearance of interesting elements—contact dispersive shock waves—that are absent in more standard, genuinely nonlinear situations. Our analytic results are confirmed by numerical simulations.

I. INTRODUCTION

The first experimental realizations of Bose-Einstein condensation of single species ultracold atomic vapors [1,2] were soon followed by their multicomponent counterparts [3] which appeared to be nontrivial extensions of the previous ones, the dynamical and nonlinear aspects of phase separation revealed to be particularly rich [4,5]. Over the years, numerous studies have been devoted to theoretical and experimental investigations associated with these specific features, namely nonlinearity and dynamics in multicomponent Bose-Einstein condensates (BECs); see, e.g., the reviews [6,7] and chapters in the books [8–10].

The specific physical ingredients of this body of research are the (intra- and interspecies) interactions, the negligible viscosity, and the large dispersive effects. Another important aspect is the different degrees of freedom associated with the different types of motion of the components. For two-component systems one can schematically separate global in-phase motion—associated with density fluctuations—from out-of-phase motion, associated with a "polarization" or "magnetic" degree of freedom. This appealing classification of the dynamical behaviors of the system is however oversimplified: in many instances, a clean separation between these idealized types of excitation is not possible, even at the perturbative level (see, e.g., the discussion in [11]). However, a recent theoretical breakthrough has been made in Ref. [12] where it has been shown that for stable two-component mixtures close to the immiscibility region, the density and magnetization degrees of freedom decouple, even at the nonlinear level. The polarization sector is particularly interesting; different solitons have been initially identified in Ref. [12] and a rich variety of nonlinear excitations rapidly followed [13]: cnoidal waves, nonlinear trigonometric waves, algebraic solitons. The interest of these studies is not uniquely theoretical: the regime of parameters for which the dynamics of polarization excitations decouples from that of density excitations corresponds to systems of experimental interest; for instance, it is exactly realized in the mixture of the two hyperfine states $|F = 1, m_F = \pm 1\rangle$ of ^{23}Na

[14], and, to a good approximation, in the mixture of hyperfine states of ^{87}Rb considered in Refs. [15] ($|1,1\rangle$ and $|2,2\rangle$) and [16] ($|1, -1\rangle$ and $|1,0\rangle$ or $|1, -1\rangle$ and $|2, -2\rangle$).

An investigation of the one-dimensional Riemann problem for polarization excitations was started in Ref. [13], which was motivated by the study of two-species counterflow considered in Ref. [15]: an initial value problem has been considered, consisting, for each component, in piecewise constant initial (relative) density and velocity, with a single discontinuity. The importance of this type of problems lies in the facts that, first, their solution involves characteristic wave patterns arising in the space-time evolution of quite general initial pulses, and, second, a number of real physical situations can be reduced to the discussion of the dynamics of initial discontinuities. The interest of this so-called "Riemann problem" was first realized in the framework of compressible fluid dynamics, where the well-known viscous shocks play a key role in the classification of evolutions of initial discontinuities (see, e.g., Ref. [17]). Extension of this approach to systems where dispersion effects play a dominant role—instead of viscous ones—started with the groundbreaking work of Gurevich and Pitaevskii [18] for the Korteweg–de Vries (KdV) equation, in which dispersive shock waves (DSWs) were approximated by nonlinear modulated waves whose evolution was described by means of Whitham theory of modulations [19,20]. The theory of DSWs has been much developed since and has found numerous different applications (see, e.g., a recent review [21] and references therein). In particular, the classification of the space-time evolution of initial discontinuities was established for waves whose dynamics is described by the nonlinear Schrödinger (NLS) equation [22,23] and by the Kaup-Boussinesq (KB) equation [24,25]. In all these cases (KdV, NLS, and KB), the evolution of the DSW is governed by the dynamical Whitham equations for the so called "Riemann invariants" [17] who have a one-to-one correspondence with relevant physical variables. However, the problem becomes much more complicated when this mapping is multivalued, even when the Whitham equations can be represented in

a diagonal form. For instance, different types of structures appear in such systems, as was indicated in Ref. [26] for the case of the modified KdV (mKdV) equation. The full solution of the Riemann problem for the Gardner equation (related with the modified KdV equation) was given in Ref. [27] and this solution was adapted to the mKdV case in Ref. [28]. These examples refer to a unidirectional wave propagation described by a single nonlinear wave equation. However, similar complicated wave structures were discussed in Ref. [29] for the nonintegrable Miyata-Camassa-Choi equation describing two-directional propagation of two-layer shallow water waves.

The case considered in Ref. [13] combines two difficulties: (i) as in the problems studied in Refs. [26–28], it corresponds to a situation where the dispersionless Riemann invariants are nonmonotonously dependent on the physical variables, that is, the problem is not *genuinely nonlinear* (see, e.g., [30]) and, (ii) as in Ref. [29], it corresponds to a two-directional wave propagation described by a system of two nonlinear equations. To avoid too many complications, the study of Ref. [13] was initially restricted to a region of parameters where the dependence of the Riemann invariants on the physical variables remains monotonous, that is, the problem considered was actually genuinely nonlinear. In the present paper we extend this study and give the full solution of the Riemann problem for the space-time evolution of polarization waves in a two-component BEC. Our approach is based on the remark made in Ref. [13] that, for the regime of parameters identified in Ref. [12], nonlinear polarization waves can be described by the dissipationless Landau-Lifshitz (LL) equation with uniaxial easy-plane anisotropy [31,32]. The exact integrability of this equation—which belongs to the Ablowitz-Kaup-Newell-Segur hierarchy—makes it possible to develop a Whitham modulational theory (Sec. IV) for describing configurations where nonlinear waves are slowly modulated, as observed in dispersive shocks. This will permit us to formulate a principle of classification valid for all the numerous wave patterns arising from the evolution of initial discontinuities.

An interesting aspect of the present work is its relevance to systems pertaining to widely different domains in physics. Configurations similar to the ones studied in the present work can be investigated in neighboring fields such as nonlinear fiber optics and also exciton-polariton condensed systems. But the physical ingredients characterizing the phenomena we are interested in—nonlinearity, weak dissipation, dispersion in a multicomponent system—are also encountered in quite different settings. As a result, the solution of the Riemann problem we give in the present work is also relevant to fluid mechanics [33–37] and to the nonlinear magnetization dynamics of anisotropic ferromagnets [38–40].

The paper is organized as follows: The model and the relevant dynamical equations are presented in Sec. II. The exact integrability of the easy-plane Landau-Lifshitz equations is used in Sec. III for writing its explicit one-phase solutions, determining the corresponding Riemann invariants, and writing the Whitham modulational equations. The full classification of the solutions of the Riemann problem is presented in Sec. V in terms of the combination of specific wave patterns, which we denote as "building blocks" or "key

elements" which are first analyzed in Sec. IV. Finally, we present our conclusions in Sec. VI.

II. MODEL

We consider a one-dimensional system consisting in an elongated two-component BEC described by the order parameters $\psi_\uparrow(x,t)$ and $\psi_\downarrow(x,t)$. The dynamics of the system is described by two coupled Gross-Pitaevskii equations:

$$\left(i\hbar\partial_t + \frac{\hbar^2\partial_x^2}{2m}\right)\begin{pmatrix}\psi_\uparrow\\\psi_\downarrow\end{pmatrix} = \begin{pmatrix} g_{\uparrow\uparrow}|\psi_\uparrow|^2 & g_{\uparrow\downarrow}\psi_\downarrow^*\psi_\uparrow \\ g_{\uparrow\downarrow}\psi_\uparrow^*\psi_\downarrow & g_{\downarrow\downarrow}|\psi_\downarrow|^2 \end{pmatrix}\begin{pmatrix}\psi_\uparrow\\\psi_\downarrow\end{pmatrix},$$

(1)

where $g_{\uparrow\uparrow}$ and $g_{\downarrow\downarrow}$ are the intraspecies nonlinear constants; $g_{\uparrow\downarrow}$ is the interspecies one. We consider the limit where $g_{\uparrow\uparrow} \approx g_{\downarrow\downarrow}$ and denote as g their common value (the situation where these two constants are not exactly equal is treated in Ref. [11]). We denote as δg the difference $g - g_{\uparrow\downarrow}$ and consider the situation

$$0 < \delta g \ll g. \qquad (2)$$

The left condition is the mean-field miscibility condition of the two species (see, e.g., Refs. [8,9]). The right condition implies that the three interaction constants are close to each other and that the system is close to the region of immiscibility. As discussed in Refs. [12,13], in this situation the density and magnetic degrees of freedom effectively decouple.

The spinor wave function is parametrized as [41]

$$\begin{pmatrix}\psi_\uparrow\\\psi_\downarrow\end{pmatrix} = \sqrt{\rho}\, e^{i\Phi/2}\, \Xi, \quad \text{where} \quad \Xi = \begin{pmatrix}\cos\theta\, e^{-i\phi/2}\\\sin\theta\, e^{i\phi/2}\end{pmatrix}. \quad (3)$$

In this expression $\rho(x,t)$ is the total density and $\theta(x,t)$ governs the relative densities of the two components: $\rho_\uparrow(x,t) = |\psi_\uparrow|^2 = \frac{1}{2}\rho(1+\cos\theta)$ and $\rho_\downarrow(x,t) = |\psi_\downarrow|^2 = \frac{1}{2}\rho(1-\cos\theta)$. $\Phi(x,t)$ and $\phi(x,t)$ are potentials for the velocity fields $v_\uparrow$ and $v_\downarrow$ of the two components, namely,

$$v_\uparrow(x,t) = \frac{\hbar}{2m}(\Phi_x - \phi_x), \quad v_\downarrow(x,t) = \frac{\hbar}{2m}(\Phi_x + \phi_x). \quad (4)$$

(Throughout the text the x and t indices denote partial derivatives, whereas numerical indices denote space components of vectors.) The small perturbations of a uniform BEC of total density ρ_0 with equal fractions of the two components ($\theta = \pi/2$) correspond to total density fluctuations which propagate with velocity $c_d = [\rho_0(g - \delta g/2)/m]^{1/2}$ and polarization excitations with velocity $c_p = (\rho_0\delta g/2m)^{1/2}$. In the limit (2) these two velocities are widely different. As a result, even an initial state consisting of a mixture of density and polarization fluctuations rapidly separates into density perturbations propagating at large velocity c_d away from a region where only polarization excitations take place. For considering these excitations, it is appropriate to rescale the lengths in units of the polarization healing length $\xi_p = \hbar/(2m\rho_0\delta g)^{1/2}$ and time in units of $\tau_p = \xi_p/c_p$. Once this is done, it has been shown in [13] that the dynamics of the polarization excitations is accounted for by the following system of coupled equations:

$$\theta_t + 2\theta_x\phi_x\cos\theta + \phi_{xx}\sin\theta = 0,$$

$$\phi_t - \cos\theta(1 - \phi_x^2) - \frac{\theta_{xx}}{\sin\theta} = 0. \qquad (5)$$

The other fields are fixed by the conditions $\rho(x,t) = \rho_0$ and $(\Phi_x - \phi_x \cos\theta)_x = 0$. Introducing the effective spin (σ_1, σ_2, and σ_3 are the Pauli matrices)

$$\mathbf{S} = \Xi^\dagger \, \boldsymbol{\sigma} \, \Xi = \begin{pmatrix} \sin\theta \cos\phi \\ \sin\theta \sin\phi \\ \cos\theta \end{pmatrix} \qquad (6)$$

and the magnetization $\mathbf{M} = -\mathbf{S}$, one can easily verify that the system of equations (5) is equivalent to the dissipationless Landau-Lifshitz equation for an easy-plane ferromagnet:

$$\partial_t \mathbf{M} = \mathbf{H}_{\text{eff}} \wedge \mathbf{M}, \quad \text{where} \quad \mathbf{H}_{\text{eff}} = \partial_x^2 \mathbf{M} - M_3 \, \mathbf{e}_3, \qquad (7)$$

$\mathbf{e}_3$ being a unit vector of the z axis. We have found that this form of the equations of motion is particularly appropriate for numerical simulations. The reason is that, contrarily to the systems (5) [and (8); see below], it does not involve small denominators when the density of one of the components gets very small. The other interesting feature of this system is that the anisotropic Landau-Lifshitz system (7) is integrable by the inverse scattering transform method and the corresponding Lax pair is known (see, e.g., [42,43]). This result has been used in Ref. [44] to derive periodic solutions for ferromagnets with an easy-axis anisotropy, and we shall adapt here this approach to the easy-plane case (7).

For future convenience, we introduce a third version of (5): Let us define the quantities $w(x,t) = \cos\theta = S_3 = -M_3 = (\rho_\uparrow - \rho_\downarrow)/\rho_0$ describing the variations of the relative density, and $v(x,t) = \phi_x = (v_\downarrow - v_\uparrow)/(2c_p)$ which represents the nondimensional relative velocity. In terms of these two fields the equations of motion read

$$w_t - [(1 - w^2)v]_x = 0,$$

$$v_t - [(1 - v^2)w]_x + \left[\frac{1}{\sqrt{1 - w^2}} \left(\frac{w_x}{\sqrt{1 - w^2}} \right)_x \right]_x = 0. \qquad (8)$$

Before embarking to the study of nonlinear phenomena, it is interesting to briefly consider linear perturbations of a stationary configuration: let a uniform background be characterized by a relative density w_0 and a relative velocity v_0. Small perturbations of the type

$$w = w_0 + w'(x,t), \; v = v_0 + v'(x,t), \; \text{with } |v'|, |w'| \ll 1$$

can be sought under the form of plane waves with wave vector k and angular frequency ω. Linearizing the system (8) one obtains the following dispersion relation:

$$\omega = \left(2w_0 v_0 \pm \sqrt{(1 - w_0^2)(1 - v_0^2) + k^2} \right) k. \qquad (9)$$

By definition we always have $|w_0| = |\cos\theta_0| \leqslant 1$, however v_0 can have any value, and for $|v_0| > 1$ the frequency ω is complex for small enough wave vectors k. This implies a long wavelength modulational instability of a system with large relative velocity of the two components, more precisely for a background relative velocity $v_\downarrow - v_\uparrow$ larger than $2c_p$. This mechanism of instability has been theoretically studied in Ref. [45].

In what follows, we consider the dynamically stable situation where $|v_0| < 1$. In this case the large wavelength limit of the dispersion relation (9) corresponds to waves propagating

with the "polarization" or "magnetization" sound velocity

$$c_\pm = 2w_0 v_0 \pm \sqrt{(1 - w_0^2)(1 - v_0^2)}. \qquad (10)$$

For a uniform system in which both components have equal densities ($w_0 = 0$) and no relative velocity ($v_0 = 0$) one gets $c_\pm = \pm 1$, i.e., going back to dimensional quantities, the speed of the magnetic sound is $\pm c_p$ as expected. We note that the $+$ sign ($-$ sign) in expression (10) corresponds to polarization excitations propagating to the right (to the left) with respect to the background in the reference frame in which the total flux of the condensate is zero.

Limiting regimes

For some specific values of the field variables, the anisotropic Landau-Lifshitz system (7) can be approximated by simpler nonlinear models. In the present subsection we consider two limiting cases: the nonlinear Schrödinger equation (Sec. II 1) and the Kaup-Boussinesq system (Sec. II 2). These limiting regimes will be used in Secs. V A and V B to help classifying the large number of different solutions of the Riemann problem.

1. Nonlinear Schrödinger regime

In the regime where $w(x,t)$ is close to unity and $v(x,t)$ is small, defining $w'(x,1) = 1 - w(x,t)$ one can rewrite the system (8) keeping only terms up to second order in the small quantities v and w':

$$w'_t + 2(w'v)_x = 0,$$

$$v_t + 2vv_x + w'_x + \left[\frac{w_x'^2}{4w'^2} - \frac{w'_{xx}}{2w'} \right]_x = 0. \qquad (11)$$

Defining $n = w'/2$ and changing variable to $T = 2t$, the system (11) can be cast in the form

$$n_T + (nv)_x = 0,$$

$$v_T + vv_x + n_x + \left[\frac{n_x^2}{8n^2} - \frac{n_{xx}}{4n} \right]_x = 0, \qquad (12)$$

which is the hydrodynamic form of the defocusing nonlinear Schrödinger equation

$$i\psi_T = -\tfrac{1}{2}\psi_{xx} + |\psi|^2 \psi. \qquad (13)$$

The system (12) is obtained from the standard form (13) by means of the Madelung transform [$n = |\psi|^2$ and $v = (\arg\psi)_x$]. We note that a similar approximation is also valid for $w(x,t)$ close to -1 and small $v(x,t)$.

2. Kaup-Boussinesq regime

In the regime where $v(x,t)$ is close to unity and $w(x,t)$ is small, defining $v'(x,t) = 1 - v(x,t)$, one can rewrite the system (8) keeping only terms up to second order in the small quantities v' and w:

$$w_t + 2ww_x + v'_x = 0,$$
$$v'_t + 2(v'w)_x - w_{xxx} = 0. \qquad (14)$$

One defines here $u = \sqrt{2}\,w$, $h = v'$ and changes the spatial variable to $X = x/\sqrt{2}$. This casts the approximate system (14)

into the canonical Kaup-Boussinesq form [46]

$$u_t + uu_X + h_X = 0,$$

$$h_t + (hu)_X - \tfrac{1}{4}u_{XXX} = 0. \quad (15)$$

Again a similar approximation can be derived when $v(x,t)$ is close to -1 and $w(x,t)$ small.

III. PERIODIC SOLUTIONS AND WHITHAM EQUATIONS

Among the key elements that are generated during the evolution of nonlinear waves, an important role is played by the DSWs that can be represented as modulated periodic solutions of the corresponding nonlinear wave equation. Consequently, for classifying the wave patterns evolving from an initial discontinuity in the polarization mode, we have to present the periodic solutions of the LL equation in the most convenient form and to derive the corresponding Whitham modulation equations.

In Ref. [13] the periodic solutions have been found by a direct method, and were not parametrized in terms of Riemann invariants. The Whitham equations were used in El's form [47] which provides the main information concerning the evolution of initial steplike discontinuous distributions without requiring the knowledge of the Riemann invariants. However, for solving the full Riemann problem it is more appropriate to use methods based on the explicit knowledge of the Riemann invariants. In this section we shall obtain the periodic solutions of the LL equation by means of the finite gap integration method, give the explicit form of the Riemann invariants, and derive the corresponding Whitham modulation equations.

A. One-phase finite-gap integration method of the easy-plane Landau-Lifshitz equation

In this subsection, relying on the finite gap integration method, we list all the traveling wave solutions of the LL equation (7) [Eqs. (39)–(52)]. These solutions are naturally parametrized in terms of the roots of the "resolvent" $\mathcal{R}$ [defined in Eq. (36)]. At the end of the subsection, and in view of the implementation of the Whitham averaging technique (Sec. III B), we relate these roots to the ones of another characteristic polynomial [P defined in Eq. (22)] formed by the squared basis functions of the associated linear problem.

As well known, the LL equation (7) is integrable by the inverse scattering transform method (see, e.g., [42,43]). The corresponding Lax pair can be written as

$$\frac{\partial}{\partial x}\begin{pmatrix} \tilde{\psi}_1 \\ \tilde{\psi}_2 \end{pmatrix} = \begin{pmatrix} F & G \\ H & -F \end{pmatrix}\begin{pmatrix} \tilde{\psi}_1 \\ \tilde{\psi}_2 \end{pmatrix}, \quad (16)$$

$$\frac{\partial}{\partial t}\begin{pmatrix} \tilde{\psi}_1 \\ \tilde{\psi}_2 \end{pmatrix} = \begin{pmatrix} A & B \\ C & -A \end{pmatrix}\begin{pmatrix} \tilde{\psi}_1 \\ \tilde{\psi}_2 \end{pmatrix}, \quad (17)$$

where

$$F = \frac{i\lambda}{2}M_3, \quad G = -\frac{1}{2}\sqrt{1-\lambda^2}M_-,$$

$$H = -\frac{1}{2}\sqrt{1-\lambda^2}M_+,$$

$$A = \frac{i}{2}(1-\lambda^2)M_3 + \frac{\lambda}{4}[(M_-)_x M_+ - M_-(M_+)_x],$$

$$B = \frac{1}{2}\lambda\sqrt{1-\lambda^2}M_- + \frac{i}{2}\sqrt{1-\lambda^2}[(M_3)_x M_- - M_3(M_-)_x],$$

$$C = \frac{1}{2}\lambda\sqrt{1-\lambda^2}M_+ - \frac{i}{2}\sqrt{1-\lambda^2}[(M_3)_x M_+ - M_3(M_+)_x]. \quad (18)$$

In (18) $M_\pm = M_1 \pm i M_2$ and λ is a constant spectral parameter. Periodic solutions for ferromagnets with an easy-axis anisotropy were found in Ref. [44] and we shall here adapt the approach used in this reference to the easy-plane case of Eq. (7). The 2×2 linear problems (16) and (17) have two linearly independent basis solutions which we denote as $(\tilde{\psi}_1, \tilde{\psi}_2)^T$ and $(\tilde{\varphi}_1, \tilde{\varphi}_2)^T$. We define the "squared basis functions"

$$f = -\frac{i}{2}(\tilde{\psi}_1\tilde{\varphi}_2 + \tilde{\psi}_2\tilde{\varphi}_1), \quad g = \tilde{\psi}_1\tilde{\varphi}_1, \quad h = -\tilde{\psi}_2\tilde{\varphi}_2, \quad (19)$$

which obey the linear equations

$$f_x = -iHg + iGh, \quad (20a)$$

$$g_x = 2iGf + 2Fg, \quad (20b)$$

$$h_x = -2iHf - 2Fh, \quad (20c)$$

and

$$f_t = -iCg + iBh, \quad (21a)$$

$$g_t = 2iBf + 2Ag, \quad (21b)$$

$$h_t = -2iCf - 2Ah. \quad (21c)$$

It is easy to check that the expression $f^2 - gh$ does not depend on x and t by virtue of Eqs. (20) and (21), however it can depend on the spectral parameter λ. The (quasi)periodic solutions are distinguished by the condition that the term $f^2 - gh$ be a polynomial $P(\lambda)$. For the one-phase case which we are interested in, it suffices to consider a fourth degree polynomial,

$$f^2 - gh = P(\lambda) = \prod_{i=1}^{4}(\lambda - \lambda_i)$$
$$= \lambda^4 - s_1\lambda^3 + s_2\lambda^2 - s_3\lambda + s_4, \quad (22)$$

where s_i are standard symmetric functions of the four zeros ($\lambda_1, \lambda_2, \lambda_3,$ and λ_4) of the polynomial:

$$s_1 = \sum_i \lambda_i, \quad s_2 = \sum_{i<j} \lambda_i\lambda_j, \quad s_3 = \sum_{i<j<k} \lambda_i\lambda_j\lambda_k,$$

$$s_4 = \lambda_1\lambda_2\lambda_3\lambda_4. \quad (23)$$

We write the solution of Eqs. (20) and (21) under the form

$$f(x,t) = M_3\lambda^2 - f_1(x,t)\lambda + f_2(x,t),$$

$$g(x,t) = M_-\sqrt{1-\lambda^2}(\lambda - \mu(x,t)), \quad (24)$$

$$h(x,t) = M_+\sqrt{1-\lambda^2}(\lambda - \mu^*(x,t)),$$

where, to simplify computations, we have chosen the coefficients of the terms with the highest degrees in λ in such a way that the identity (22) is already satisfied at order λ^4. The quantities $f_1(x,t)$, $f_2(x,t)$, $\mu(x,t)$, and $\mu^*(x,t)$ in (24) are yet unknown functions; $\mu(x,t)$ and $\mu^*(x,t)$ are *a priori* unrelated,

but we shall soon establish that they are complex conjugate one to the other, hence the notation.

Plugging expressions (24) back into (22) and equating the coefficients of the powers of λ yields four conservation laws:

$$-2f_1 w + (1 - w^2)(\mu + \mu^*) = s_1,$$
$$2f_1 f_2 - (1 - w^2)(\mu + \mu^*) = s_3,$$
$$f_1^2 - 2f_2 w + (1 - w^2)(\mu\mu^* - 1) = s_2,$$
$$f_2^2 - (1 - w^2)\mu\mu^* = s_4, \qquad (25)$$

where we have used the above defined notation $w \equiv -M_3$ and have also taken into account the normalization

$$M_+ M_- + M_3^2 = 1. \qquad (26)$$

Substitution of (24) into (20) and (21) gives, after equating the coefficients of powers of λ, a number of differential equations; we shall write down here the ones which are the most important for our purpose. For instance Eq. (20a) gives

$$w_x = -\frac{i}{2}(1 - w^2)(\mu - \mu^*), \quad f_{1,x} = 0, \quad f_{2,x} = w_x. \quad (27)$$

After factoring out the term $\sqrt{1 - \lambda^2}$, the equality of the coefficients of the terms of order λ in both sides of Eq. (20b) yields

$$(M_-)_x / M_- = i(f_1 + w\mu). \qquad (28)$$

This equation, with account of $\phi_x = v$, $M_- = -\sqrt{1 - w^2} \exp(-i\phi)$, and of the first of Eqs. (27), leads to the following expression for the relative velocity:

$$v = -f_1 - \frac{1}{2}(\mu + \mu^*)w. \qquad (29)$$

The variable μ satisfies the equation

$$\mu_x = i\sqrt{P(\mu)}, \qquad (30)$$

which can be easily obtained by putting the free parameter λ equal to μ in Eq. (20b). Substitution of (28) and (27) into (21b) where the parameter λ is taken equal to μ gives, owing to the first of identities (25), the equation $\mu_t = -(i/2)s_1 \sqrt{P(\mu)} = -(1/2)s_1 \mu_x$. This indicates that μ depends on the variable $\xi = x - (s_1/2)t$ only, that is

$$\mu_\xi = i\sqrt{P(\mu)}, \quad \xi = x - Vt, \quad V = \frac{1}{2}s_1. \qquad (31)$$

Formally, Eq. (31) can be solved in terms of elliptic functions and it is then parametrized by the zeros of the polynomial $P(\lambda)$. However, even for given values of these zeros, the trajectory of μ in the complex μ plane is not known and therefore it is impossible to prescribe the initial value of μ without some additional study. This difficulty can be overcome by the method suggested in Ref. [48], according to which the parameters f_1, f_2, μ, μ^* are to be represented as functions of w. This yields the solution in a so-called "effective" form, not subject to any additional constraint.

After simple manipulations on the system (25), we find, for a given set of λ_i ($i = 1,2,3,4$), four possible forms of f_1:

$$f_1 = \pm\sqrt{(1 + s_2 + s_4 + s_4')/2}, \qquad (32a)$$

and

$$f_1 = \pm\mathrm{sgn}(s_1 + s_3)\sqrt{(1 + s_2 + s_4 - s_4')/2}, \qquad (32b)$$

where we have defined

$$\lambda_i' = \sqrt{1 - \lambda_i^2}, \quad s_4' = \lambda_1'\lambda_2'\lambda_3'\lambda_4', \qquad (33)$$

and made use of the identity $(1 + s_2 + s_4)^2 - (s_1 + s_3)^2 = (s_4')^2$. The factor $\mathrm{sgn}(s_1 + s_3)$ is introduced for making f_1 (and its derivatives with respect to λ_i) continuous functions of λ_i. For f_2 we obtain in all cases

$$f_2 = (s_1 + s_3)/2f_1 + w, \qquad (34)$$

and the variables μ, μ^* are given by the expressions

$$\mu, \mu^* = \frac{s_1 + 2f_1 w \pm 2i\sqrt{-\mathcal{R}(w)}}{2(1 - w^2)}, \qquad (35)$$

where

$$\mathcal{R}(w) = w^4 + \frac{s_1 + s_3}{f_1}w^3 + s_2 w^2 + \left(f_1 s_1 - \frac{s_1 + s_3}{f_1}\right)w$$
$$+ \frac{1}{4}(s_1^2 - 4 - 4s_2 + 4f_1^2). \qquad (36)$$

Since μ depends on ξ only, the same holds for w, which, as follows from Eqs. (27) and (35), satisfies the equation

$$w_\xi = \sqrt{-\mathcal{R}(w)}. \qquad (37)$$

This equation admits a real solution when w oscillates between two of the zeros of $\mathcal{R}(w)$ (provided they both are located in the interval $[-1,1]$), in a domain where $\mathcal{R}(w) \leqslant 0$, and in this case, on sees from (35) that μ and μ^* are complex conjugated variables, as was anticipated earlier.

Actually, Eq. (37) coincides with Eq. (30) of Ref. [13] [with $Q(w)$ replaced by $\mathcal{R}(w)$] and we shall reproduce here briefly its solutions for convenience and future references. We denote the zeros of $\mathcal{R}$ as $w_1 \leqslant w_2 \leqslant w_3 \leqslant w_4$.

(a) We first consider the periodic solution corresponding to oscillations of w in the interval

$$w_1 \leqslant w \leqslant w_2. \qquad (38)$$

In this case the solution of Eq. (37) can be written as

$$w = w_2 - \frac{(w_2 - w_1)\mathrm{cn}^2(W, m)}{1 + \frac{w_2 - w_1}{w_4 - w_2}\mathrm{sn}^2(W, m)}, \qquad (39)$$

where it is assumed that $w(0) = w_1$,

$$W = \sqrt{(w_3 - w_1)(w_4 - w_2)}\,\xi/2, \qquad (40)$$

and

$$m = \frac{(w_4 - w_3)(w_2 - w_1)}{(w_4 - w_2)(w_3 - w_1)}, \qquad (41)$$

cn and sn being Jacobi elliptic functions [49]. The wavelength of the oscillating function (39) is

$$L = \frac{4K(m)}{\sqrt{(w_3 - w_1)(w_4 - w_2)}}, \qquad (42)$$

where $K(m)$ is the complete elliptic integral of the first kind [49]. In the limit $w_3 \to w_2$ ($m \to 1$) the wavelength tends to

infinity and the solution (39) transforms to a soliton

$$w = w_2 - \frac{w_2 - w_1}{\cosh^2 W + \frac{w_2 - w_1}{w_4 - w_2}\sinh^2 W}. \quad (43)$$

This is a "dark soliton" for the variable w.

The limit $m \to 0$ can be reached in two ways.

(i) If $w_2 \to w_1$, then we get

$$w \cong w_2 - \tfrac{1}{2}(w_2 - w_1)\cos[k(x - Vt)],$$
$$k = \sqrt{(w_3 - w_1)(w_4 - w_1)}. \quad (44)$$

This is a small-amplitude limit describing propagation of a harmonic wave.

(ii) If $w_4 = w_3$ but $w_1 \neq w_2$, then we get a nonlinear wave represented in terms of trigonometric functions:

$$w = w_2 - \frac{(w_2 - w_1)\cos^2 W}{1 + \frac{w_2 - w_1}{w_3 - w_2}\sin^2 W},$$
$$W = \sqrt{(w_3 - w_1)(w_3 - w_2)}\,\xi/2. \quad (45)$$

If we take the limit $w_2 - w_1 \ll w_3 - w_1$ in this solution, then we return to the small-amplitude limit (44) with $w_4 = w_3$. On the other hand, if we take here the limit $w_2 \to w_3 = w_4$, then the argument of the trigonometric functions becomes small and we can approximate them by the first terms of their series expansions. This corresponds to an algebraic soliton of the form

$$w = w_2 - \frac{w_2 - w_1}{1 + (w_2 - w_1)^2(x - Vt)^2/4}. \quad (46)$$

(b) In the second case, the variable w oscillates in the interval

$$w_3 \leqslant w \leqslant w_4. \quad (47)$$

Here again, a standard calculation yields

$$w = w_3 + \frac{(w_4 - w_3)\mathrm{cn}^2(W,m)}{1 + \frac{w_4 - w_3}{w_3 - w_1}\mathrm{sn}^2(W,m)}, \quad (48)$$

with the same definitions (40), (41), and (42) for W, m, and L, respectively, and $w(0) = w_4$. In the soliton limit $w_3 \to w_2$ ($m \to 1$) we get

$$w = w_2 + \frac{w_4 - w_2}{\cosh^2 W + \frac{w_4 - w_2}{w_2 - w_1}\sinh^2 W}. \quad (49)$$

This is a "bright soliton" for the variable w.

Again, the limit $m \to 0$ can be reached in two ways.

(i) If $w_4 \to w_3$, then we obtain a small-amplitude harmonic wave

$$w \cong w_3 + \tfrac{1}{2}(w_4 - w_3)\cos[k(x - Vt)],$$
$$k = \sqrt{(w_3 - w_1)(w_3 - w_1)}. \quad (50)$$

This is a small-amplitude limit describing a harmonic wave.

(ii) If $w_2 = w_1$, then we obtain another nonlinear trigonometric solution,

$$w = w_3 + \frac{(w_4 - w_3)\cos^2 W}{1 + \frac{w_4 - w_3}{w_3 - w_1}\sin^2 W},$$
$$W = \sqrt{(w_3 - w_1)(w_4 - w_1)}\,\xi/2. \quad (51)$$

If we assume that $w_4 - w_3 \ll w_4 - w_1$, then this reproduces the small-amplitude limit (50) with $w_2 = w_1$. On the other hand, in the limit $w_3 \to w_2 = w_1$ we obtain the algebraic soliton solution:

$$w = w_1 + \frac{w_4 - w_1}{1 + (w_4 - w_1)^2(x - Vt)^2/4}. \quad (52)$$

The solutions presented above are parametrized by the zeros w_i ($i = 1,2,3,4$) of the polynomial (36) whose coefficients are expressed in terms of the zeros λ_i of the polynomial $P(\lambda)$ which plays a key role in the finite-gap integration method. As we shall see, the parameters λ_i represent the Riemann invariants in the Whitham modulation theory. We want to express the solutions of (37) in terms of these Riemann invariants: we therefore need to express the w_i's in terms of the λ_i's explicitly, without having to solve the algebraic equation $\mathcal{R}(w) = 0$. This has been already achieved in Ref. [44], but we shall derive here expressions under a form which is more convenient for subsequent applications. To this end, we rewrite the identity (22) using explicit formulas for the functions f, g, and h:

$$P(\lambda) = \left(-w\lambda^2 - f_1\lambda + \frac{s_1 + s_3}{2f_1} + w\right)^2$$
$$- (1 - w^2)(1 - \lambda^2) \times \left[\lambda - \frac{s_1 + 2f_1 w + 2\sqrt{\mathcal{R}(w)}}{2(1 - w^2)}\right]$$
$$\times \left[\lambda - \frac{s_1 + 2f_1 w - 2\sqrt{\mathcal{R}(w)}}{2(1 - w^2)}\right].$$

Let $\lambda = \lambda_i$ be a zero of the polynomial $P(\lambda)$ and w be also one of the zeros of $\mathcal{R}(w)$. Then, for a given w, the above identity yields two equations,

$$-w\lambda_i^2 - f_1\lambda_i + \frac{s_1 + s_3}{2f_1} + w$$
$$= \pm\sqrt{1 - w^2}\,\lambda_i'\left[\lambda_i - \frac{s_1 + 2f_1 w}{2(1 - w^2)}\right],$$

for the four roots λ_i. We assume that λ_1 and λ_2 correspond to the upper sign and that λ_3 and λ_4 correspond to the lower sign. We temporarily introduce the notation

$$N_i = 2f_1 w\lambda_i' + (s_1 + s_3 - 2f_1^2\lambda_i)/\lambda_i' = 2f_1\lambda_i'w + \tilde{s}_i, \quad (53)$$

where $\tilde{s}_i$ is a notation for $(s_1 + s_3 - 2f_1^2\lambda_i)/\lambda_i'$. The use of formulas (32) for f_1 yields

$$\tilde{s}_i = (s_1 - \lambda_i)\lambda_i' + s_4\frac{\lambda_i'}{\lambda_i} \mp s_4'\frac{\lambda_i}{\lambda_i'}, \quad (54)$$

where the upper sign corresponds to Eq. (32a), and the lower one to Eq. (32b). It is then possible to rewrite Eq. (53) under the form

$$N_i = \pm\frac{f_1}{\sqrt{1 - w^2}}[2\lambda_i(1 - w^2) - s_1 - 2f_1 w]. \quad (55)$$

Dividing expressions (55) for the N_i's one by the other for various pairs of i and j ($\neq i$), we get

$$\frac{N_i}{N_j} = \pm\frac{2\lambda_i(1 - w^2) - s_1 - 2f_1 w}{2\lambda_j(1 - w^2) - s_1 - 2f_1 w},$$

where the plus signs applies for N_1/N_2 and N_3/N_4 and the minus one for the other choices of these pairs. Consequently we have

$$1 - w^2 = \frac{s_1 + 2 f_1 w}{2} \frac{N_i \pm N_j}{\lambda_j N_i \pm \lambda_i N_j} \qquad (56)$$

with the same sign convention. Equating these expressions for $1 - w^2$ to each other, we obtain a number of equations—linear and quadratic in the N_i's. For example, from the equality

$$\frac{N_1 + N_2}{\lambda_2 N_1 + \lambda_1 N_2} = \frac{N_2 - N_3}{\lambda_3 N_2 - \lambda_2 N_3} \qquad (57)$$

we get the first relationship of the system,

$$(\lambda_3 - \lambda_2)N_1 + (\lambda_3 - \lambda_1)N_2 - (\lambda_2 - \lambda_1)N_3 = 0,$$
$$(\lambda_3 - \lambda_2)N_1 + (\lambda_3 - \lambda_1)N_2 + (\lambda_2 - \lambda_1)N_3 = 0,$$
$$(\lambda_3 - \lambda_2)N_1 - (\lambda_3 - \lambda_1)N_2 + (\lambda_2 - \lambda_1)N_3 = 0,$$
$$(\lambda_3 - \lambda_2)N_1 - (\lambda_3 - \lambda_1)N_2 - (\lambda_2 - \lambda_1)N_3 = 0, \qquad (58)$$

and the three others can be obtained by considering equalities of the type (57) for other choices of pairs of indices. Although these equations are not linearly independent (one can check that one of them is a linear combination of the other three), we prefer to deal with all of them to get symmetrical expressions for all four roots of the resolvent. Indeed, using the expression (53) for N_i, each of the relationships (58) becomes a linear equation for w and yields one of the zeros of the polynomial $\mathcal{R}(w)$. As a result we obtain the formulas

$$w_1 = -\frac{1}{2 f_1} \frac{(\lambda_3 - \lambda_2)\tilde{s}_1 + (\lambda_3 - \lambda_1)\tilde{s}_2 - (\lambda_2 - \lambda_1)\tilde{s}_3}{(\lambda_3 - \lambda_2)\lambda_1' + (\lambda_3 - \lambda_1)\lambda_2' - (\lambda_2 - \lambda_1)\lambda_3'},$$

$$w_2 = -\frac{1}{2 f_1} \frac{(\lambda_3 - \lambda_2)\tilde{s}_1 + (\lambda_3 - \lambda_1)\tilde{s}_2 + (\lambda_2 - \lambda_1)\tilde{s}_3}{(\lambda_3 - \lambda_2)\lambda_1' + (\lambda_3 - \lambda_1)\lambda_2' + (\lambda_2 + \lambda_1)\lambda_3'},$$

$$w_3 = -\frac{1}{2 f_1} \frac{(\lambda_3 - \lambda_2)\tilde{s}_1 - (\lambda_3 - \lambda_1)\tilde{s}_2 - (\lambda_2 - \lambda_1)\tilde{s}_3}{(\lambda_3 - \lambda_2)\lambda_1' - (\lambda_3 - \lambda_1)\lambda_2' - (\lambda_2 - \lambda_1)\lambda_3'},$$

$$w_4 = -\frac{1}{2 f_1} \frac{(\lambda_3 - \lambda_2)\tilde{s}_1 - (\lambda_3 - \lambda_1)\tilde{s}_2 + (\lambda_2 - \lambda_1)\tilde{s}_3}{(\lambda_3 - \lambda_2)\lambda_1' - (\lambda_3 - \lambda_1)\lambda_2' + (\lambda_2 - \lambda_1)\lambda_3'}, \qquad (59)$$

where the w_i's are ordered according to $w_1 \leqslant w_2 \leqslant w_3 \leqslant w_4$ under the suppositions that $\lambda_1 \leqslant \lambda_2 \leqslant \lambda_3 \leqslant \lambda_4$ and $f_1 > 0$. A change of sign of f_1 leads to a simple reordering of the expressions for the w_i's. We see that the zeros λ_i of the polynomial $P(\lambda)$ and the zeros w_i of the polynomial $\mathcal{R}(w)$ are related by the symmetrical formulas (59), therefore we shall call $\mathcal{R}(w)$ the resolvent of the polynomial $P(\lambda)$ (for example, in the case of NLS equation an analogous method yields the well-known Ferrari cubic resolvent used for solving in radicals fourth degree algebraic equations). Formulas (59) are equivalent to those obtained in Ref. [44], however they are more convenient for the study of degenerate cases presented below. It is important to note that we have four values of f_1 for each set of the λ_i's [and corresponding values (54) for $\tilde{s}_i$], which are thus mapped by the formulas (59) to four sets of w_i's. This multiplicity of mappings will prove of tremendous importance when applying the Whitham theory of modulations to the representations (39) and (48) of the periodic solutions. Before addressing this crucial question we first need to demonstrate that the parameters λ_i ($i = 1, 2, 3, 4$) are the

Riemann invariants of the Whitham system for the averaged conservation laws. This is achieved in the next section.

B. Whitham equations

In modulated waves the λ_i's become slowly varying functions of the space and time variables and their evolution is governed by the Whitham modulation equations. Whitham showed in Refs. [19,20] that these equations can be obtained by averaging the conservation laws of the full nonlinear system over fast oscillations (whose wavelength L changes slowly along the total wave pattern). Generally speaking, in cases where the periodic solution is characterized by four parameters, this averaging procedure leads to a system of four equations of the type $w_{i,t} + \sum_j v_{ij}(w_1, w_2, w_3, w_4) w_{j,x} = 0$ with 16 entries of the "velocity matrix" v_{ij}. However, the Landau-Lifshitz equation being completely integrable, this system of four equations reduces to a diagonal "Riemann form" for the λ_i's, similarly to what occurs for the usual Riemann invariants of nondispersive waves (see, e.g., Ref. [17]). As a result, the λ_i's are called the Riemann invariants of the dispersive nonlinear wave. We shall study their properties by using the method devised in Refs. [50,51].

First of all, we notice that Eq. (35) implies that, during the oscillations of w, the variable μ describes a cycle in the complex plane which encloses either points λ_1 and λ_2 or points λ_3 and λ_4 [according to Eq. (30) the variable μ runs along one of the two loops of an hyperelliptic curve while the w variable oscillates within the corresponding interval]. Hence, from Eq. (31) one can derive the following expression for the wavelength:

$$L = \oint \frac{d\mu}{\sqrt{-P(\mu)}} = \frac{4K(m)}{\sqrt{(\lambda_3 - \lambda_1)(\lambda_4 - \lambda_2)}}. \qquad (60)$$

Comparison of this expression with Eq. (42) leads to the identities

$$m = \frac{(w_4 - w_3)(w_2 - w_1)}{(w_4 - w_2)(w_3 - w_1)} = \frac{(\lambda_4 - \lambda_3)(\lambda_2 - \lambda_1)}{(\lambda_4 - \lambda_2)(\lambda_3 - \lambda_1)}, \qquad (61)$$

and

$$(w_4 - w_2)(w_3 - w_1) = (\lambda_4 - \lambda_2)(\lambda_3 - \lambda_1). \qquad (62)$$

From (20b) and (21b) and owing to the normalization condition (26) one gets $B g_x - G g_t = 2(BF - AG)g = \frac{1}{2}\sqrt{1 - \lambda^2}[i M_3 M_- + \lambda(M_-)_x]g$. Using the equations of motion (7) this last term can be rewritten as $g G_t - g B_x$. Dividing by g^2, one can cast the resulting identity under the form

$$\frac{\partial}{\partial t}\left(\sqrt{P(\lambda)}\frac{G(\lambda)}{g(\lambda)}\right) - \frac{\partial}{\partial x}\left(\sqrt{P(\lambda)}\frac{B(\lambda)}{g(\lambda)}\right) = 0. \qquad (63)$$

We shall use this equation as the generating function of the conservation laws of the Landau-Lifshitz equation: a series expansion in inverse powers of λ gives an infinite number of conservation laws of this completely integrable system. The factor $\sqrt{P(\lambda)}$ has been introduced to transform the identity (22) to the form

$$\left(\frac{f}{\sqrt{P(\lambda)}}\right)^2 - \frac{g}{\sqrt{P(\lambda)}}\frac{h}{\sqrt{P(\lambda)}} = 1,$$

so that the right-hand side is independent of the variations of λ_i in a modulated wave, hence the densities and fluxes in the conservation laws can change due to modulations only, as it should be, and any changes caused by λ-dependent normalization of the f,g,h functions are excluded.

Substitution of Eqs. (18) and (24) into (63) and its simple transformation with the use of Eqs. (25) and (28) gives

$$\frac{\partial}{\partial t}\left(\frac{\sqrt{P(\lambda)}}{\lambda-\mu}\right)+\frac{\partial}{\partial x}\left[\sqrt{P(\lambda)}\left(1+\frac{s_1/2}{\lambda-\mu}\right)\right]=0.$$

Averaging of the density and of the flux in this expression over one wavelength L (60) yields the generating function of the *averaged* conservation laws:

$$\frac{\partial}{\partial t}\left[\frac{\sqrt{P(\lambda)}}{L}\oint\frac{d\mu}{(\lambda-\mu)\sqrt{-P(\mu)}}\right]$$
$$+\frac{\partial}{\partial x}\left[\frac{\sqrt{P(\lambda)}}{L}\oint\left(1+\frac{s_1/2}{\lambda-\mu}\right)\frac{d\mu}{\sqrt{-P(\mu)}}\right]=0. \quad (64)$$

The condition that in the limit $\lambda\to\lambda_i$ the singular terms cancel yields

$$\oint\frac{d\mu}{(\lambda_i-\mu)\sqrt{-P(\mu)}}\frac{\partial\lambda_i}{\partial t}$$
$$+\left(L+\frac{s_1}{2}\oint\frac{d\mu}{(\lambda_i-\mu)\sqrt{-P(\mu)}}\right)\frac{\partial\lambda_i}{\partial x}=0. \quad (65)$$

From the definition (60) of L one obtains

$$\oint\frac{d\mu}{(\lambda_i-\mu)\sqrt{-P(\mu)}}=-2\frac{\partial L}{\partial\lambda_i},$$

which makes it possible to cast Eq. (65) under the form of a Whitham equation for the variables λ_i:

$$\frac{\partial\lambda_i}{\partial t}+v_i\frac{\partial\lambda_i}{\partial x}=0, \quad (66)$$

where the Whitham velocity v_i is given by

$$v_i=\frac{s_1}{2}-\frac{L}{2\partial L/\partial\lambda_i}, \quad \text{for} \quad i\in\{1,2,3,4\}. \quad (67)$$

By means of Eq. (60) one obtains the following explicit expressions:

$$v_1=\frac{1}{2}\sum_{i=1}^4\lambda_i-\frac{(\lambda_4-\lambda_1)(\lambda_2-\lambda_1)K(m)}{(\lambda_4-\lambda_1)K(m)-(\lambda_4-\lambda_2)E(m)},$$

$$v_2=\frac{1}{2}\sum_{i=1}^4\lambda_i+\frac{(\lambda_3-\lambda_2)(\lambda_2-\lambda_1)K(m)}{(\lambda_3-\lambda_2)K(m)-(\lambda_3-\lambda_1)E(m)},$$

$$v_3=\frac{1}{2}\sum_{i=1}^4\lambda_i-\frac{(\lambda_4-\lambda_3)(\lambda_3-\lambda_2)K(m)}{(\lambda_3-\lambda_2)K(m)-(\lambda_4-\lambda_2)E(m)},$$

$$v_4=\frac{1}{2}\sum_{i=1}^4\lambda_i+\frac{(\lambda_4-\lambda_2)(\lambda_4-\lambda_1)K(m)}{(\lambda_4-\lambda_1)K(m)-(\lambda_3-\lambda_1)E(m)},$$

$$(68)$$

where $K(m)$ and $E(m)$ are complete elliptic integrals of the first and second kind, respectively.

In a modulated wave representing a DSW, the Riemann invariants change with x and t. The DSW occupies a region in
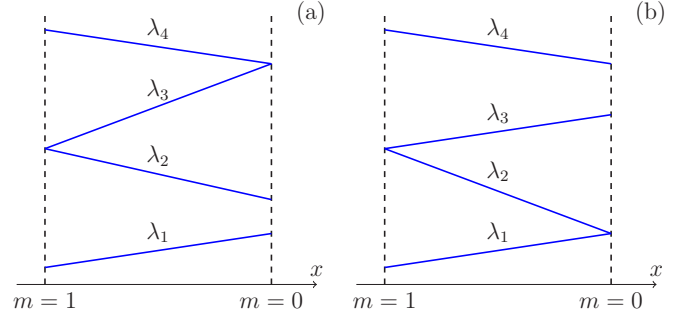

FIG. 1. Sketches of the space dependence of the Riemann invariants along a DSW. In both cases the limit $\lambda_2=\lambda_3$ corresponds to the soliton edge. The polarity of the solitons depends on the choice of solution of formulas (59) by which the solution of the Whitham equations are mapped onto the parameters w_i. The small amplitude edge corresponds to $\lambda_3=\lambda_4$ in case (a) and to $\lambda_1=\lambda_2$ in case (b).

space at the edges of which two Riemann invariants coincide. There are two possible situations represented schematically in Fig. 1. In both cases the soliton edge corresponds to $\lambda_3=\lambda_2$ ($m=1$) and at this edge the Whitham velocities are given by

$$v_1=\tfrac{1}{2}(3\lambda_1+\lambda_4), \quad v_2=v_3=\tfrac{1}{2}(\lambda_1+2\lambda_2+\lambda_4),$$
$$v_4=\tfrac{1}{2}(\lambda_1+3\lambda_4), \quad \text{for} \quad \lambda_3=\lambda_2. \quad (69)$$

The small amplitude limit $m=0$ can be obtained in two ways. If $\lambda_3=\lambda_4$ [Fig. 1(a)], then we get

$$v_1=\frac{1}{2}(3\lambda_1+\lambda_2), \quad v_2=\frac{1}{2}(\lambda_1+3\lambda_2),$$
$$v_3=v_4=2\lambda_4+\frac{(\lambda_2-\lambda_1)^2}{2(\lambda_1+\lambda_2-2\lambda_4)}, \quad (70)$$

and if $\lambda_2=\lambda_1$ [Fig. 1(b)], then

$$v_1=v_2=2\lambda_1+\frac{(\lambda_4-\lambda_3)^2}{2(\lambda_3+\lambda_4-2\lambda_1)},$$
$$v_3=\frac{1}{2}(3\lambda_3+\lambda_4), \quad v_4=\frac{1}{2}(\lambda_3+3\lambda_4). \quad (71)$$

As one can see from Eqs. (59), for $\lambda_2=\lambda_1$ we have $w_2=w_1$ and for $\lambda_3=\lambda_4$ we have $w_3=w_4$. Consequently, Eqs. (70) and (71) represent also the Whitham velocities for evolution of shocks approximated by the trigonometric solutions (51) and (45), respectively. We shall call them "trigonometric shocks." As we shall see, they play an important role in the classification of the possible wave structures evolving from initial discontinuities.

We can now proceed to the description of key elements ("building blocks") from which the wave patterns are constructed.

IV. KEY ELEMENTS

The Riemann problem we consider in the present work consists in the study of the time evolution of an initial steplike

structure of the form

$$w(x,t=0) = \begin{cases} w_L & \text{if } x < 0, \\ w_R & \text{if } x > 0, \end{cases}$$

$$v(x,t=0) = \begin{cases} v_L & \text{if } x < 0, \\ v_R & \text{if } x > 0. \end{cases} \quad (72)$$

We consider the hyperbolic case where the four boundary values w_L, w_R, v_L, and v_R are contained in the interval $[-1,1]$. The initial distribution involves no characteristic constants having the dimension of a length or a time, however the system (8) has soliton solutions and the width of these solitons can be considered as a characteristic length, of order unity (in dimensioned units, it is of order of the polarization healing length ξ_p). Nevertheless, if we consider nonlinear structures at a much larger scale, as is the case for modulated waves whose envelopes change little over a wavelength, then we can neglect such a "microscopic" length scale and look for smooth solutions of the Whitham equations. In short: at the "macroscopic" scale there is no characteristic length in the initial conditions (72) and the solutions of the Whitham equations can be sought as functions of the self-similar variable $z = x/t$ only.

There exist also smooth solutions of the original system (8) in which not the envelopes, but the functions $w(x,t)$ and $v(x,t)$ themselves depend slowly on the space coordinate. This corresponds to a hydrodynamic regime in which one can neglect the higher derivatives in the second equation of the system (8). Again, such hydrodynamic approximate solutions can only depend on the self-similar variable $z = x/t$. These smooth nondispersive waves can contribute—as DSWs do—to the whole wave structures arising from the space-time evolution of the initial profiles (72).

It is convenient, in a first stage, to select particular initial conditions for which the time evolved wave structure reduces to a single type of wave (hydrodynamic, modulated cnoidal, modulated trigonometric, etc.). In a second step (Sec. V) we will proceed to the full classification of the structures evolving from arbitrary initial conditions, but in the present section we shall first identify what we denote as "key elements," solutions of the Riemann problem for specific values of the boundary value constants. These are the building blocks of which are composed the general self-similar solution of the Riemann problem. We shall start with the hydrodynamic key elements which are solutions for which dispersive effects can be neglected.

A. Plateau and rarefaction waves

As stated above, nonlinear polarization waves with typical length scale much larger than unity can be described in the framework of a dispersionless treatment in which the dispersive term in (8) is omitted:

$$w_t - [(1 - w^2)v]_x = 0, \quad v_t - [(1 - v^2)w]_x = 0. \quad (73)$$

We shall denote these equations as *Bellevaux-Ovsyannikov equations* since they were first obtained independently by these authors in the theory of two-layer shallow water dynamics [33,34] (see also [35–37]).

First of all, we note that these equations have a simple solution

$$w(x,t) = \overline{w} = \text{const}, \quad v(x,t) = \overline{v} = \text{const}. \quad (74)$$

In spite of its "triviality," such a solution can play an important role as an element of a complex self-similar structure. In this context, this flow is limited to a finite region of space, whose edge points (say x_+ and x_-) move with constant velocities $s_\pm = x_\pm/t$ (see below). We shall call such an expanding region of constant flow a "plateau region."

Now, since both variables w and v depend on the single variable z, they can be considered as functions of each other and, hence, such self-similar solutions are denoted as "simple wave" solutions of the hydrodynamic equations (73); see, e.g., Ref. [52]. For their study it is convenient to transform the Bellevaux-Ovsyannikov system to a diagonal Riemann form by defining the Riemann invariants [35],

$$r_\pm = vw \pm \sqrt{(1-v^2)(1-w^2)}. \quad (75)$$

As a result we obtain the system

$$\partial_t r_\pm + v_\pm(r_-, r_+)\,\partial_x r_\pm = 0, \quad (76)$$

where $v_\pm$ are the "Riemann velocities,"

$$\begin{aligned} v_- &= \tfrac{3}{2}r_- + \tfrac{1}{2}r_+ = 2vw - \sqrt{(1-v^2)(1-w^2)}, \\ v_+ &= \tfrac{1}{2}r_- + \tfrac{3}{2}r_+ = 2vw + \sqrt{(1-v^2)(1-w^2)}. \end{aligned} \quad (77)$$

Equations (76) are reminiscent of the equations of compressible gas dynamics; see, e.g., Refs. [17,51]. We note here that, although the relative density $w(x,t) = \cos\theta(x,t)$ is constrained to vary between -1 and 1, the relative velocity $v(x,t)$ can assume, generally speaking, any values (as will be exemplified in Secs. V A and V B). However, in the regime we consider here, because of the assumption of slow variation of the field $v(x,t)$, a value larger than 1 (or lower than -1) suffers from a dynamical instability because it induces perturbations which grow exponentially (as in the uniform case discussed in Sec. II), resulting in oscillations which cannot be treated within the dispersionless approximation. The Riemann variables (75) are thus always properly defined only in the "hyperbolicity region"

$$-1 \leqslant v, w \leqslant 1, \quad (78)$$

where the velocities (77) are real.

One can also remark that the Riemann velocities (77) expressed in terms of v and w correspond to the sound velocity (10) for a uniform background characterized by w and v, in agreement with the long wavelength approximation which is at the heart of the dispersionless approximation.

For a simple wave solution, one of the Riemann invariants is constant, and this condition [namely, either $r_-(v,w) = \text{const}$ or $r_+(v,w) = \text{const}$] gives, when applied to Eq. (75), the above mentioned relationship between the variables v and w. Consequently, on the (v,w) plane these simple wave solutions are depicted as arcs of the ellipse $(r_\pm - vw)^2 = (1-v^2)(1-w^2)$ or

$$\frac{(v+w)^2}{2(1+r)} + \frac{(v-w)^2}{2(1-r)} = 1, \quad (79)$$
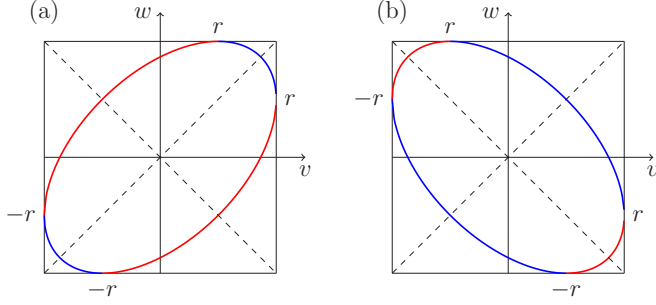
FIG. 2. Simple-wave solutions in the (v,w) plane. Along these branches of ellipse only one Riemann invariant varies; the value of the constant other one is denoted by r. In (a) we have $r > 0$ and in (b) $r < 0$. Red arcs correspond to $r_+ = $ const and blue ones to $r_- = $ const.

where r denotes the constant value of r_+ or r_-. This ellipse is inscribed into a square $-1 \leqslant w,v \leqslant 1$ [domain of hyperbolicity; cf. (78)] and touches its sides at four points with coordinates

$$(1,r), \quad (-1,-r), \quad (-r,-1), \quad \text{and} \quad (r,1). \tag{80}$$

If $r_- + r_+ \geqslant 0$ (i.e., when w and v have the same sign), the physical variables are expressed in terms of the Riemann invariants by the formulas

$$w = \pm\sqrt{\tfrac{1}{2}\big[1 + r_-r_+ \pm \sqrt{(1-r_-^2)(1-r_+^2)}\big]},$$

$$v = \pm\sqrt{\tfrac{1}{2}\big[1 + r_-r_+ \mp \sqrt{(1-r_-^2)(1-r_+^2)}\big]}. \tag{81}$$

Otherwise, for $r_- + r_+ \leqslant 0$ (i.e., when w and v have opposite signs),

$$w = \pm\sqrt{\tfrac{1}{2}\big[1 + r_-r_+ \pm \sqrt{(1-r_-^2)(1-r_+^2)}\big]},$$

$$v = \mp\sqrt{\tfrac{1}{2}\big[1 + r_-r_+ \mp \sqrt{(1-r_-^2)(1-r_+^2)}\big]}. \tag{82}$$

It is clear that in the expressions (81) and (82) one should have $|r_\pm| \leqslant 1$.

On the ellipses (79) we can express w as a function of v in an explicit form. To do so, it is convenient to distinguish four arcs and to write

$$w(v) = \begin{cases} r_+v + \sqrt{(1-r_+^2)(1-v^2)}, & -1 \leqslant v \leqslant r_+ = \mathrm{C^{st}}, \\ r_+v - \sqrt{(1-r_+^2)(1-v^2)}, & -r_+ = \mathrm{C^{st}} \leqslant v \leqslant 1, \\ r_-v - \sqrt{(1-r_-^2)(1-v^2)}, & -1 \leqslant v \leqslant -r_- = \mathrm{C^{st}}, \\ r_-v + \sqrt{(1-r_-^2)(1-v^2)}, & r_- = \mathrm{C^{st}} \leqslant v \leqslant 1. \end{cases}$$
$$\tag{83}$$

In Fig. 2 the arcs for constant r_- are shown in blue and those for constant r_+ in red. The value of the constant is denoted as r. On these arcs, the Riemann invariant which varies reaches its maximal value (equal to 1) on the diagonal $w = v$ (for r_+) or on the antidiagonal $w = -v$ (for r_-); at the end points—whose coordinates are listed in (80)—it is equal to r.

The dependence of w and v on the self-similar variable $z = x/t$ is found at once by noticing that in this case the system (76) reduces to

$$(v_- - z)\frac{dr_-}{dz} = 0, \quad (v_+ - z)\frac{dr_+}{dz} = 0. \tag{84}$$

Hence, if one of the Riemann invariants is constant, the Riemann velocity of the other must be equal to z. Thus we arrive at two possible solutions $r_- = $ const, $v_+ = x/t \equiv z$ and $r_+ = $ const, $v_- = x/t \equiv z$. Let us consider the first one in some detail. It is characterized by the relations

$$v_+ = \frac{1}{2}r_- + \frac{3}{2}r_+ = z = \frac{x}{t}, \quad r_- = \text{const.} \tag{85}$$

More explicitly, we have two equations,

$$v_+ = 2vw + \sqrt{(1-v^2)(1-w^2)} = z,$$

$$r_- = vw - \sqrt{(1-v^2)(1-w^2)} = \text{const},$$

which yield

$$w(z) = \pm\big\{\tfrac{1}{6}\big[3 + 2r_-z - r_-^2$$
$$\pm 2\sqrt{(1-r_-^2)(z - \tfrac{1}{2}r_- + \tfrac{3}{2})(\tfrac{1}{2}r_- + \tfrac{3}{2} - z)}\big]\big\}^{1/2}, \tag{86}$$

and

$$v(z) = \frac{r_- + z}{3\,w(z)}. \tag{87}$$

The solution has thus four branches—corresponding to four possible choices of signs in (86)—that are located within the interval

$$\tfrac{1}{2}r_- - \tfrac{3}{2} \leqslant z \leqslant \tfrac{1}{2}r_- + \tfrac{3}{2}. \tag{88}$$

Comparing (88) and (85) one sees that at the end points we have $r_+ = \pm 1$. The four branches of the solutions are represented in Fig. 3. It is important to stress that the solution expressed in terms of the Riemann invariants by Eq. (85) is mapped into four arcs in the (v,w) plane and four functions $w = w(z)$ given by Eq. (86).

Similar formulas and plots can be obtained for the solution $r_+ = $ const, $v(r_-,r_+) = x/t \equiv z$.

The simplest concrete situation of physical interest is represented in Fig. 4(a). It consists in the path in the (v,w) plane formed by a single arc AB which corresponds to a rarefaction wave shown in Fig. 4(b). This arc is described by the last of formulas (83). Here the initial jump (72) in the relative density evolves into a smooth rarefaction wave, similarly to what occurs in the "dam break problem" in compressible fluid dynamics when a gas expands into vacuum flowing along a tube after removal of a wall. At the initial state both components are at rest, $v_L = v_R = 0$, the total density is fixed, i.e., $\rho_\uparrow + \rho_\downarrow = 1$ everywhere and does not change with time, and initially we have $\rho = \rho_\uparrow^L = 1$ for $x < 0$, $\rho = \rho_\uparrow^R < 1$ for $x > 0$. This means that we have a "vacuum" of the component $\rho_\downarrow$ for $x < 0$ at the initial time. The value of the constant Riemann invariant is fixed by the parameters of the flow at point A: $r_- = -\sqrt{1 - w_R^2} = -2\sqrt{\rho_\uparrow^R(1 - \rho_\uparrow^R)}$. The parameters of the flow at the matching point A preserve their values during the time evolution and therefore $r_+(A) = \sqrt{1 - w_R^2} = -r_-$.
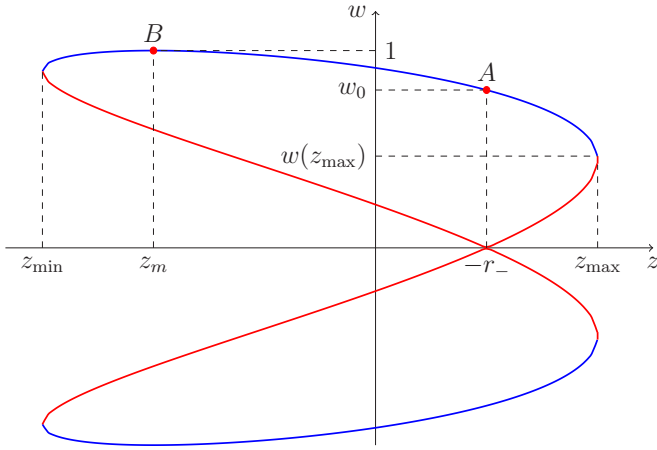
FIG. 3. Dispersionless simple-wave solutions $w(z)$ plotted as functions of $z = x/t$. The figure is drawn for $r_- = $ const. This constant value is expressed by means of (75) in terms of two constants, $w_0 > 0$ and $v_0 = 0$, i.e., $r_- = -\sqrt{1 - w_0^2} < 0$ and $w_0 = \sqrt{1 - r_-^2}$. Here $z_{max} = \frac{1}{2}r_- + \frac{3}{2}$, $w(z_{max}) = \sqrt{(1 + r_-)/2}$, $z_{min} = \frac{1}{2}r_- - \frac{3}{2}$, and $w(z_{min}) = \sqrt{(1 - r_-)/2}$. The value $w = 1$ is reached for $z = z_m = 2r_- = -2\sqrt{1 - w_0^2}$. The arc between points A and B is used below for constructing an "expansion into vacuum" solution; see Fig. 4.

Consequently, this edge of the rarefaction wave propagates to the right at a velocity $s_+ = [r_- + 3r_+(A)]/2 = -r_- = \sqrt{1 - w_R^2} = 2\sqrt{\rho_\uparrow^R(1 - \rho_\uparrow^R)}$, which coincides with the polarization sound velocity (10) in this case. At point B we have $w(B) = 1$, hence $r_+(B) = v(B) = r_- = -\sqrt{1 - w_R^2}$, and this edge propagates to the left with velocity $s_- = [r_- + 3r_+(B)]/2 = 2r_- = \sqrt{1 - w_R^2} = -4\sqrt{\rho_\uparrow^R(1 - \rho_\uparrow^R)}$. As we see, this is not the sound velocity of waves in the component $\rho_\uparrow$, but rather the maximal velocity of expansion of the component $\rho_\downarrow$ into its vacuum. This quasi-one-dimensional flow of two-component BEC was studied numerically in Ref. [15] and analytically in Ref. [13].

In the above solution, the rarefaction wave connects two plateaus with parameters $v_L = r_-$, $w_L = 1$ and $v_R = 0$, $w_R = \sqrt{1 - r_-^2}$, in such a way that the Riemann invariant r_- is
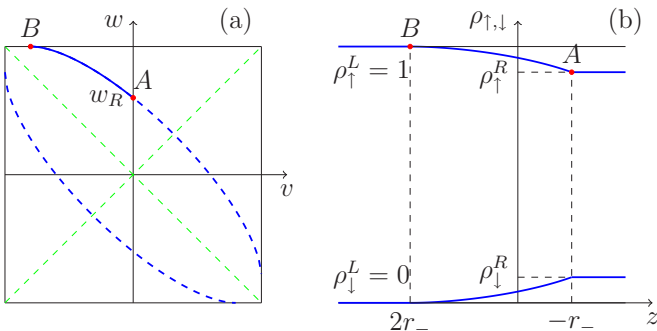

FIG. 4. (a) The solid blue arc represents a simple-wave solution with $w_L = 1$, $w_R > 0$, and $v_R = v_L = 0$ in the (v, w) plane. (b) Corresponding density profiles $\rho_{\uparrow,\downarrow}$ plotted as functions of $z = x/t$.
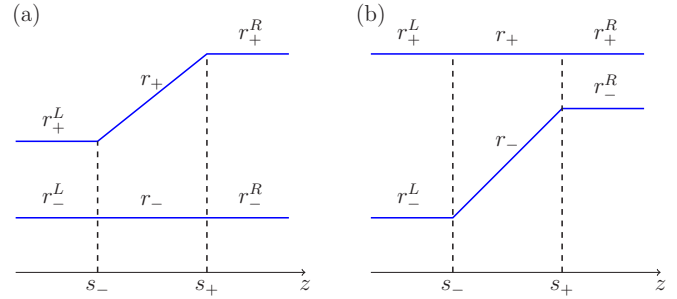

FIG. 5. Sketches of the behavior of the Riemann invariants in rarefaction wave solutions of the hydrodynamic equations with boundary conditions (89): (a) $r_- = $ const, $r_+^L < r_+^R$; (b) $r_+ = $ const, $r_-^L < r_-^R$.

constant along the wave and the plateaus. It is clear that this solution can be generalized to any rarefaction waves connecting two plateaus provided the following two conditions are fulfilled. First, one of the Riemann invariants must have the same value on both plateaus,

$$\text{(a)} \quad r_-^L = r_-^R \quad \text{or} \quad \text{(b)} \quad r_+^L = r_+^R. \quad (89)$$

Second, since the one of the Riemann invariants which varies is a solution of type (85) which depends monotonously on z, the dependence of the Riemann invariants in terms of the physical parameters must also be monotonous in order to keep the solution single valued. This means that the two edge points of the rarefaction wave must lie within one of the four triangles which are obtained by cutting the hyperbolicity square by its diagonals along which the Riemann invariants reach their extremal values. We shall denote these triangles as *monotonicity triangles*. They play an important role in the classification of the wave patterns because they define the domains where the characteristic velocities (77) satisfy the conditions of genuine nonlinearity (see, e.g., Ref. [30]). Besides that, both edge points must lie on the same branch of the ellipse and should not be separated by a point where the ellipse touches a side of the hyperbolicity square (the four sides of this square correspond to $v = \pm 1$ and $w \in [-1, 1]$ or $w = \pm 1$ and $v \in [-1, 1]$). For these rarefaction wave solutions, the behavior of the Riemann invariants considered as functions of z is displayed in Fig. 5. The edge velocities of the rarefaction waves are equal to

$$\text{(a)} \quad s_- = \tfrac{1}{2}r_-^L + \tfrac{3}{2}r_+^L, \quad s_+ = \tfrac{1}{2}r_-^R + \tfrac{3}{2}r_+^R;$$
$$\text{(b)} \quad s_- = \tfrac{3}{2}r_-^L + \tfrac{1}{2}r_+^L, \quad s_+ = \tfrac{3}{2}r_-^R + \tfrac{1}{2}r_+^R. \quad (90)$$

As we shall see in the next sections, such rarefaction waves are among the key elements from which a generic wave pattern may be composed. Obviously, their observation implies that $r_+^L < r_+^R$ in case (a) or $r_-^L < r_-^R$ in case (b), which imposes conditions on the parameters of the initial discontinuity. It is natural to ask what happens if the boundary conditions correspond to opposite inequalities (namely $r_+^L > r_+^R$ or $r_-^L > r_-^R$); this question leads us to the study of another type of key element—dispersive shock waves.
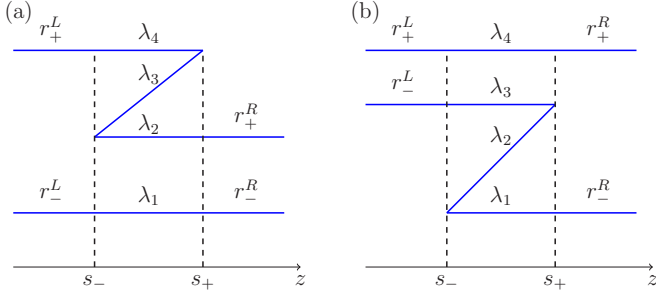
FIG. 6. Sketches of the behavior of the Riemann invariants in DSW solutions of the Whitham equations with the boundary conditions (a) $r_-^L = r_-^R, r_+^L > r_+^R$ or (b) $r_+^L = r_+^R, r_-^L > r_-^R$.

B. Cnoidal dispersive shock waves

If we try naively to use a formal self-similar solution of the type (85) for describing a wave satisfying boundary conditions such that $r_+^L > r_+^R$ or $r_-^L > r_-^R$, then we arrive at once to physically meaningless multivalued solutions (see, e.g., [51]) which represent the simplest wave breaking situation. In this case, the major insight of Gurevich and Pitaevskii [18] has been to take into account the dispersive effects which lead to the generation of oscillations in regions where the physical variables have large spatial derivatives: the multivalued solution must be replaced by a modulated nonlinear periodic solution whose parameters satisfy the Whitham equations (at least for large enough evolution time). As a matter of fact, this oscillating wave structure replaces the well-known shock waves occurring in viscous compressible fluid dynamics and hence it is called a *dispersive shock wave* (DSW).

From a formal point of view, we look again for self-similar solutions, here not for the equations (76), but instead for the Whitham equations (66). Assuming in these equations that the λ's depend only on the variable $z = x/t$ we obtain at once

$$\{v_i(\lambda) - z\}\frac{d\lambda_i}{dz} = 0, \quad i = 1,2,3,4. \tag{91}$$

In the case where the Whitham velocities are given by Eq. (68), one can satisfy this system if three Riemann invariants remain constant while the fourth one varies in such a way that the expression in the curly brackets vanishes. We assume that at both its edges the DSW matches with a smooth solution of the hydrodynamic equations and therefore at these edges the averaged equations should reproduce the same dynamics as the dispersionless hydrodynamic equations do. The comparison of the limiting expressions (69)–(71) with the diagonal form of the hydrodynamic equations (76) and (77) shows that the matching conditions can be satisfied if the Riemann invariants behave as represented in Fig. 6. It is clear that wave structures of this type appear only if the flows at the edges of the DSW satisfy either the condition (a) $r_-^L = r_-^R$ or (b) $r_+^L = r_+^R$ which coincide with (89). According to Fig. 6, the three constant Riemann invariants in the solutions of the Whitham equations are determined by the boundary conditions and the z dependence of the remaining one is determined by the vanishing of the expression in curly brackets in

Eqs. (91):

$$\begin{aligned}
\text{(a)} \quad & \lambda_1 = r_-^L, \quad \lambda_2 = r_+^R, \quad \lambda_4 = r_+^L, \\
& v_3(r_-^L, r_+^R, \lambda_3(z), r_+^L) = z; \\
\text{(b)} \quad & \lambda_1 = r_-^R, \quad \lambda_3 = r_-^L, \quad \lambda_4 = r_+^L, \\
& v_2(r_-^R, \lambda_2(z), r_-^L, r_+^L) = z.
\end{aligned} \tag{92}$$

These formulas show that the edge velocities of the DSW are unambiguously determined by the values of the Riemann invariants at its boundaries. They are equal to

$$\begin{aligned}
\text{(a)} \quad & s_- = \frac{1}{2}(r_-^L + 2r_+^R + r_+^L), \\
& s_+ = 2r_+^L + \frac{(r_+^R - r_-^R)^2}{2(r_+^R + r_-^R - 2r_+^L)}; \\
\text{(b)} \quad & s_- = 2r_+^R + \frac{(r_+^L - r_-^L)^2}{2(r_+^L + r_-^L - 2r_+^R)}, \\
& s_+ = \frac{1}{2}(r_-^R + 2r_+^L + r_+^R).
\end{aligned} \tag{93}$$

However, the situation changes in what concerns the envelopes of the DSWs, because the mapping (59) of the λ's to the physical parameters (v,w) is multivalued. As a result, each of the λ diagrams in Figs. 6(a) or 6(b) corresponds to four different DSWs. To clearly see this, let us consider the limiting expressions of Eqs. (59) at the edges of the DSW.

We first assume that $f_1 > 0$ is given by Eq. (32a). Then, after some calculations, we obtain for the case of Fig. 6(a), at the soliton edge with $\lambda_3 = \lambda_2$, the expressions

$$w_1 = -\sqrt{\frac{1}{2}\left[1 + \left(2\lambda_2^2 - 1\right)S_{1,4}^{(+)} - 2\lambda_2\lambda_2'E_{1,4}^{(-)}\right]}, \tag{94a}$$

$$w_2 = w_3 = -\sqrt{\frac{1}{2}(1 + \lambda_1\lambda_4 - \lambda_1\lambda_4')}, \tag{94b}$$

$$w_4 = \sqrt{\frac{1}{2}\left[1 + \left(2\lambda_2^2 - 1\right)S_{1,4}^{(+)} + 2\lambda_2\lambda_2'E_{1,4}^{(-)}\right]}, \tag{94c}$$

where, for shortening the formulas, we have introduced the notations

$$S_{i,j}^{(\pm)} = \lambda_i\lambda_j \pm \lambda_i'\lambda_j', \quad \text{and} \quad E_{i,j}^{(\pm)} = \lambda_i\lambda_j' \pm \lambda_i'\lambda_j. \tag{95}$$

At the small amplitude edge with $\lambda_3 = \lambda_4$ one obtains

$$w_1 = -\sqrt{\frac{1}{2}\left[1 + \left(2\lambda_4^2 - 1\right)S_{1,2}^{(+)} - 2\lambda_4\lambda_4'E_{1,2}^{(-)}\right]}, \tag{96a}$$

$$w_2 = -\sqrt{\frac{1}{2}\left[1 + \left(2\lambda_4^2 - 1\right)S_{1,2}^{(+)} + 2\lambda_4\lambda_4'E_{1,2}^{(-)}\right]}, \tag{96b}$$

$$w_3 = w_4 = \sqrt{\frac{1}{2}(1 + \lambda_1\lambda_2 - \lambda_1\lambda_2')}. \tag{96c}$$

If we change the sign of f_1, then, for $f_1 < 0$, these expressions will also change sign with appropriate reordering.

In a similar way, for the case of Fig. 6(a) and when $f_1 > 0$ is given by Eq. (32b), we obtain at the soliton edge with $\lambda_3 = \lambda_2$

the expressions

$$w_1 = -\sqrt{\tfrac{1}{2}\big[1 + (2\lambda_2^2 - 1)S_{1,4}^{(-)} + 2\lambda_2\lambda_2'E_{1,4}^{(+)}\big]}, \quad (97a)$$

$$w_2 = w_3 = -\sqrt{\tfrac{1}{2}(1 + \lambda_1\lambda_4 + \lambda_1\lambda_4')}, \quad (97b)$$

$$w_4 = \sqrt{\tfrac{1}{2}\big[1 + (2\lambda_2^2 - 1)S_{1,4}^{(-)} - 2\lambda_2\lambda_2'E_{1,4}^{(+)}\big]}, \quad (97c)$$

and at the small amplitude edge with $\lambda_3 = \lambda_4$ the expressions

$$w_1 = w_2 = -\sqrt{\tfrac{1}{2}(1 + \lambda_1\lambda_2 + \lambda_1\lambda_2')}. \quad (98a)$$

$$w_3 = -\sqrt{\tfrac{1}{2}\big[1 + (2\lambda_4^2 - 1)S_{1,2}^{(-)} + 2\lambda_4\lambda_4'E_{1,2}^{(+)}\big]}, \quad (98b)$$

$$w_4 = \sqrt{\tfrac{1}{2}\big[1 + (2\lambda_4^2 - 1)S_{1,2}^{(-)} - 2\lambda_4\lambda_4'E_{1,2}^{(+)}\big]}. \quad (98c)$$

Again, if we change the sign of f_1 then, for $f_1 < 0$, these expressions also change signs with appropriate reordering.

We now consider the diagram of Fig. 6(b) and assume that $f_1 > 0$ is given by Eq. (32a). Then we obtain at the soliton edge with $\lambda_3 = \lambda_2$ the expressions

$$w_1 = \sqrt{\tfrac{1}{2}\big[1 + (2\lambda_3^2 - 1)S_{1,4}^{(+)} - 2\lambda_3\lambda_3'E_{1,4}^{(-)}\big]}, \quad (99a)$$

$$w_2 = w_3 = \sqrt{\tfrac{1}{2}(1 + \lambda_1\lambda_4 - \lambda_1\lambda_4')}, \quad (99b)$$

$$w_4 = \sqrt{\tfrac{1}{2}\big[1 + (2\lambda_3^2 - 1)S_{1,4}^{(+)} + 2\lambda_3\lambda_3'E_{1,4}^{(-)}\big]}, \quad (99c)$$

and at the small amplitude edge with $\lambda_2 = \lambda_1$ the expressions

$$w_1 = w_2 = -\sqrt{\tfrac{1}{2}(1 + \lambda_3\lambda_4 - \lambda_3\lambda_4')}, \quad (100a)$$

$$w_3 = \sqrt{\tfrac{1}{2}\big[1 + (2\lambda_1^2 - 1)S_{3,4}^{(+)} - 2\lambda_1\lambda_1'E_{3,4}^{(-)}\big]}, \quad (100b)$$

$$w_4 = \sqrt{\tfrac{1}{2}\big[1 + (2\lambda_1^2 - 1)S_{3,4}^{(+)} + 2\lambda_1\lambda_1'E_{3,4}^{(-)}\big]}. \quad (100c)$$

If we take $f_1 < 0$ then these expressions will also change their signs with appropriate reordering.

At last, for the case of Fig. 6(b), when $f_1 > 0$ is given by Eq. (32b), we obtain at the soliton edge with $\lambda_3 = \lambda_2$ the expressions

$$w_1 = -\sqrt{\tfrac{1}{2}\big[1 + (2\lambda_3^2 - 1)S_{1,4}^{(-)} + 2\lambda_3\lambda_3'E_{1,4}^{(+)}\big]}, \quad (101a)$$

$$w_2 = w_3 = -\sqrt{\tfrac{1}{2}(1 + \lambda_1\lambda_4 + \lambda_1\lambda_4')}, \quad (101b)$$

$$w_4 = \sqrt{\tfrac{1}{2}\big[1 + (2\lambda_3^2 - 1)S_{1,4}^{(-)} - 2\lambda_3\lambda_3'E_{1,4}^{(+)}\big]}, \quad (101c)$$

and at the small amplitude edge with $\lambda_2 = \lambda_1$ the expressions

$$w_1 = w_2 = -\sqrt{\tfrac{1}{2}(1 + \lambda_3\lambda_4 + \lambda_3\lambda_4')}. \quad (102a)$$

$$w_3 = -\sqrt{\tfrac{1}{2}\big[1 + (2\lambda_1^2 - 1)S_{3,4}^{(-)} + 2\lambda_1\lambda_1'E_{3,4}^{(+)}\big]}, \quad (102b)$$

$$w_4 = \sqrt{\tfrac{1}{2}\big[1 + (2\lambda_1^2 - 1)S_{3,4}^{(-)} - 2\lambda_1\lambda_1'E_{3,4}^{(+)}\big]}. \quad (102c)$$

If $f_1 < 0$ then these expressions will also change their signs with appropriate reordering.
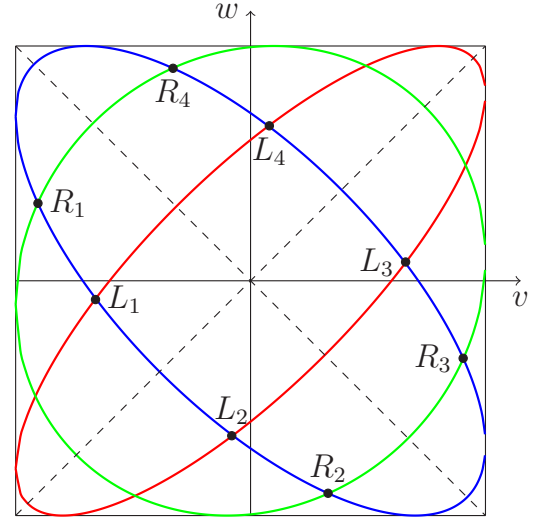

FIG. 7. Plots of the ellipses of the (v,w) plane along which the Riemann invariants $r_-^L = r_-^R = -0.7$ (blue), $r_+^L = 0.8$ (red), and $r_+^R = 0.1$ (green) are constant. Their crossing points define possible values of (v,w) at the edges of the DSWs.

Thus we see indeed that each diagram in Fig. 6 corresponds to four different sets of values for the w_i's. It is important to notice that for each set, the edges of these DSWs match with plateaus and assume limiting values coinciding with the dispersionless expressions (81) or (82). To avoid possible confusion, it is worth noticing that the above limiting expressions are correct not only for the self-similar situation but also for the general case schematically represented in Fig. 1.

It is convenient to symbolize the occurrence of a DSW by a diagram in the (v,w) plane. Let us consider for instance a possible DSW corresponding to Fig. 6(a). The equal Riemann invariants $r_-^L = r_-^R$ both correspond to the ellipse (79) represented in Fig. 7 by a blue line. Its intercepts with the ellipse corresponding to the constant r_+^L—shown in red—represent possible values of v_L and w_L at the left (soliton) edge; its intercepts with the ellipse corresponding to the constant r_+^R—shown in green—represent possible values of v_R and w_R at the right (small amplitude) edge. As we see in the figure, we get four possible pairs of boundary conditions leading to cnoidal dispersive shocks having all the same edge velocities but describing different physical situations. In particular, w_L in L_1 is given by Eq. (94b) with $\lambda_1 = r_-^L = r_-^R$, $\lambda_4 = r_+^L$, and w_R in R_1 by Eq. (96c) with $\lambda_1 = r_-^L = r_-^R$, $\lambda_2 = r_+^L$. It is important to notice that each pair of boundary points (L_3 and R_3, say) is located within a triangle obtained by cutting the hyperbolicity square by its diagonals. It means that a cnoidal DSW is possible only if both its edge points belong to the same monotonicity triangle (region of genuine nonlinearity, earlier defined in Sec. IV A). Since the edge points of the DSW belong to an ellipse of constant Riemann invariant, we can *schematically* represent each DSW by an arc of this ellipse in the (v,w) plane. But we should keep in mind that—at variance with the dispersionless situation—the actual plot representing how v and w evolve within a DSW displays large oscillations and noticeably departs from this ellipse, with which it has only the edge points in common.
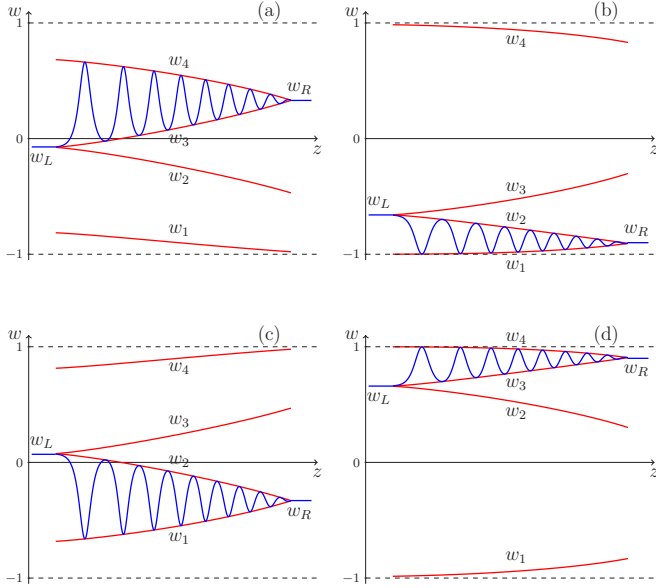
FIG. 8. Plots of the functions $w_i(z)$ (red) and of the associated dispersive shock waves (blue) corresponding to the diagram Fig. 6(a) and to the four possible choices of f_1 in Eqs. (32). In each case, two of the $w_i(z)$'s are the envelopes of the oscillatory structure, either w_1 and w_2 or w_3 and w_4, as is clear from Eqs. (39) and (48).

FIG. 9. Dispersive shock wave evolving from an initial discontinuity with parameters corresponding to the points L_1, R_1 in Fig. 7, with $r_-^L = r_-^R = -0.7$, $r_+^L = 0.8$, $r_+^R = 0.1$, which corresponds to $v_L = -0.659$, $w_L = -0.076$, $v_R = -0.906$, and $w_R = 0.331$. The edge velocities are equal to $s_- = 0.15$ and $s_+ = 1.45$. The analytic solution determined within the Whitham approximation scheme is shown by a blue line and the corresponding envelope functions by dashed black lines. The numerical solution computed for an evolution time $t = 100$ is shown by a red line. According to our definition $v = (v_\downarrow - v_\uparrow)/(2c_p)$, and the wave structure with these parameters propagates to the right.

The substitution of the solutions (92) into (59) gives the dependence of the w_i's in term of z. Since we have four sets of formulas corresponding to the four different choices of f_1 [Eqs. (32a) and (32b)], each of the two solutions (a) and (b) in (92) corresponds to four possible oscillatory behaviors for the DSW. The plots of the functions $w_i(z)$ produced by the diagram Fig. 6(a) are shown in Fig. 8: cases (a) and (b) correspond to the positive signs in Eqs. (32) and to arcs L_1R_1 and L_2R_2 in Fig. 7; cases (c) and (d) correspond to the negative signs in Eqs. (32) and to arcs L_3R_3 and L_4R_4 in Fig. 7. Obviously, the plots 8(c) and 8(d) can be obtained from the plots 8(a) and 8(b) by the transformation $w \to -w$. It is worth noticing that if we exchange the left and right boundary conditions, then the time evolution of the initial flow yields to the formation, not of a DSW, but of a rarefaction wave, such as considered in the previous subsection. In Fig. 9 we compare the analytic solution in the Whitham approximation with the exact numerical solution of the Landau-Lifshitz system for the case shown in Fig. 8(a), with $v_L = -0.659$, $w_L = -0.076$, $v_R = -0.906$, and $w_R = 0.331$, which corresponds to $r_-^L = r_-^R = -0.7$, $r_+^L = 0.8$, and $r_+^R = 0.1$. One can see that the envelope functions resulting from the Whitham approach (dashed lines) agree very well with the exact numerical solution.

In a similar way, the diagram Fig. 6(b) with $r_+^L = r_+^R$ produces four other wave structures which correspond to four arcs connecting the crossing points of the red and green ellipses in Fig. 7. Since this case does not differ essentially from the above presented one, we shall not discuss it further.

The DSWs studied in the present subsection, as the rarefaction waves presented in Sec. IV A, can serve as key elements involved in the description of a general wave structure evolving from the initial conditions (72). They can be observed
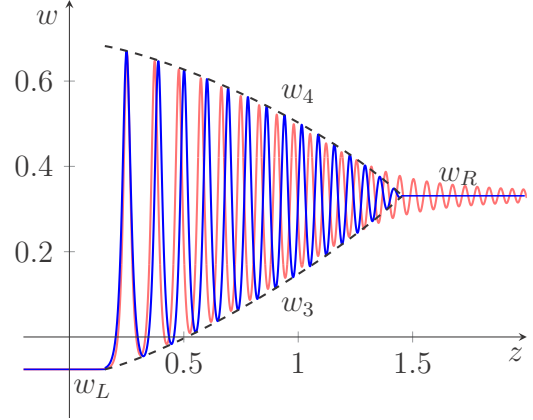
alone, in their genuine form, only if the points corresponding to the left and right boundaries belong to the same triangle of monotonicity. The transitions between two triangles imply one more element, *contact dispersive shocks*, and related structures which we consider in the next section.

C. Contact dispersive shock waves

We now turn to the study of the situation where the left and right boundary points belong to different monotonicity triangles. In this case the problem is no longer genuinely nonlinear. We shall start by studying the simplest possible configuration in which the Riemann invariants have equal values at both edges of the shock, i.e., when $r_-^L = r_-^R$, and $r_+^L = r_+^R$. This situation resembles the one of the so called "contact discontinuities" which play an important role in the theory of viscous shocks (see, e.g., Ref. [17]); therefore we shall denote the wave structures arising in this case as *contact dispersive shock waves* (CDSWs). (To avoid any confusion, we should mention that in the dynamics of immiscible condensates, interfaces between two components may appear which play the same role as the one played by contact discontinuities in the theory of viscous shocks; see, e.g., Ref. [53].) In the case of a CDSW the "left" and "right" ellipses of constant Riemann invariants in the (v,w) plane coincide with each other; cf. Fig. 10. The intersections of the ellipses $r_-^{(L,R)} = \text{const}$ and $r_+^{(L,R)} = \text{const}$ define four points denoted as A_1, A_2, B_1, and B_2 in Fig. 10. These points can refer to either the left or the right edge depending on the choice of f_1.

First of all, we should determine the generic behavior of the Riemann invariants in the case of interest here, and draw diagrams representing the solutions of the Whitham equations equivalent to the ones displayed in Figs. 5 and 6. To be definite,
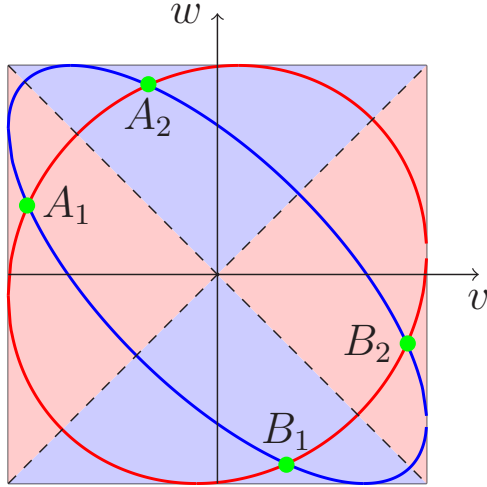
FIG. 10. Plots of the ellipses of the (v,w) plane along which the Riemann invariants $r_-^L = r_-^R = -0.7$ (red) and $r_+^L = r_+^R = 0.1$ (blue) are constant. Their crossing points define possible values of (v,w) at the edges of the contact dispersive shock.

let us consider the example represented in Fig. 10, with a left edge corresponding to point A_1, and a right one to B_1. In this case, the arc of ellipse connecting the end points crosses the main diagonal $w = v$ of the hyperbolicity square along which one of the dispersionless Riemann invariants takes its maximal value, equal to unity: $r_+ = 1$. This means that in the formal dispersionless solution, the invariant r_+ would first increase and reach its maximal value $r_+ = 1$, then decrease down to the initial value $r_+^R = r_+^L$ along the same "path" $r_+ = \frac{2}{3}(z - 2r_-^L)$ [cf. Eq. (85)]. By analogy with the case of a regular cnoidal shock considered in the preceding subsection, it is natural to assume that the actual behavior of the Riemann invariants λ_i corresponding to the Whitham equations reproduces here also the same qualitative structure as the one expected on the basis of the dispersionless analysis. This leads in the present case to the situation depicted in Fig. 11(a), where the invariants λ_1 and λ_2 remain constant within the shock region (and match the boundary conditions: $\lambda_1 = r_-^L = r_-^R$, $\lambda_2 = r_+^L = r_+^R$), whereas the two other Riemann invariants
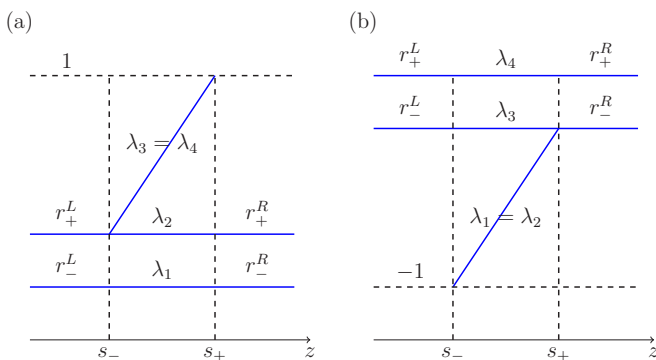

FIG. 11. Sketches of the behavior of the Riemann invariants in contact dispersive shock wave solutions of the Whitham equations with the boundary conditions (a) $r_-^L = r_-^R$ or (b) $r_+^L = r_+^R$.

are equal ($\lambda_3 = \lambda_4$) and satisfy the same Whitham equation $v_3(r_-^L, r_+^L, \lambda_4, \lambda_4) = v_4(r_-^L, r_+^L, \lambda_4, \lambda_4) = z$ [with v_3 and v_4 given by the appropriate version of Eq. (70)]. We thus get

$$\lambda_1 = r_-^L = r_-^R, \quad \lambda_2 = r_+^L = r_+^R,$$

$$v_3 = v_4 = 2\lambda_4 + \frac{(r_+^L - r_-^L)^2}{2(r_+^L + r_-^L - 2\lambda_4)} = z, \tag{103}$$

where the last formula determines the dependence of λ_4 on z, which can be presented in an explicit form

$$\lambda_4(z) = \tfrac{1}{4}[z + r_+^L + r_-^L + \sqrt{(z - r_+^L - r_-^L)^2 + 2(r_+^L - r_-^L)^2}]. \tag{104}$$

Here z varies within the interval $s_- \leqslant z \leqslant s_+$ with

$$s_- = \frac{3r_+^L + r_-^L}{2}, \quad s_+ = 2 + \frac{(r_+^L - r_-^L)^2}{2(r_+^L + r_-^L - 2)}. \tag{105}$$

The wavelength in this case is given by the formula

$$L = \frac{2\pi}{\sqrt{[\lambda_4(z) - r_-^L][\lambda_4(z) - r_+^L]}}. \tag{106}$$

Substitution of this solution into Eqs. (96) yields the dependence of the parameters w_i on z which, in turn, determines—according to Eq. (51)—the oscillatory structure of $w(x,t)$ in a different type of shock which we shall call, as mentioned above, a contact dispersive shock wave.

In a similar way, we may consider the diagram represented in Fig. 11(b) which corresponds in the (v,w) plane to paths crossing the antidiagonal $w = -v$. The solution of the Whitham equations takes the form [see Eq. (71)]

$$v_1 = v_2 = 2\lambda_1 + \frac{(r_+^L - r_-^L)^2}{2(r_+^L + r_-^L - 2\lambda_1)} = z,$$

$$\lambda_3 = r_-^L = r_-^R, \quad \lambda_4 = r_+^L = r_+^R, \tag{107}$$

or

$$\lambda_1(z) = \tfrac{1}{4}[z + r_+^L + r_-^L - \sqrt{(z - r_+^L - r_-^L)^2 + 2(r_+^L - r_-^L)^2}] \tag{108}$$

where z belongs to the interval $s_- \leqslant z \leqslant s_+$ with

$$s_- = -2 + \frac{(r_+^L - r_-^L)^2}{2(r_+^L + r_-^L + 2)}, \quad s_+ = \frac{r_+^L + 3r_-^L}{2}. \tag{109}$$

The wavelength is here given by the formula

$$L = \frac{2\pi}{\sqrt{[\lambda_1(z) - r_-^L][\lambda_1(z) - r_+^L]}}. \tag{110}$$

Now, as in the case of cnoidal DSWs, we have to determine how these solutions of the Whitham equations are mapped onto the envelop parameters w_i. For example, if we take $f_1 > 0$ given by Eq. (32a), then in the limit $m \to 0$ these parameters are presented by the formulas (96) and w oscillates in the interval $w_1 \leqslant w \leqslant w_2$ leading to the trigonometric modulated wave (45). This situation is depicted in Fig. 12(a). Obviously, it corresponds to the transition $A_1 \to B_1$ in the (v,w) plane. At the soliton edge with $\lambda_4 = \lambda_2$ we obtain for the parameters
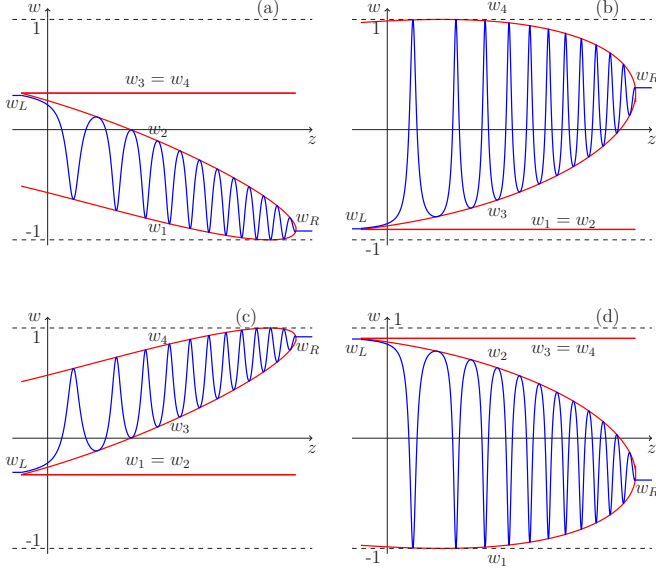
FIG. 12. Contact dispersive shock waves (blue) and associated envelope functions w_i (red) describing the solution of the Whitham equations which is represented by the diagram shown in Fig. 11(a) with $r_-^L = r_-^R = -0.7$, $r_+^L = r_+^R = 0.1$. The four shocks correspond to the four possible choices for the parameter f_1 in Eqs. (32).
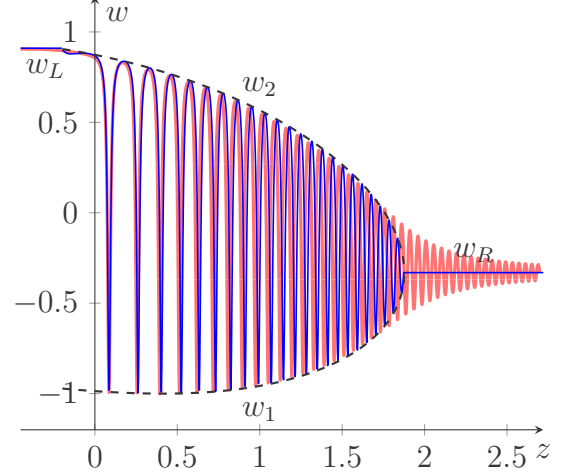

FIG. 13. Comparison of the Whitham analytic solution shown in Fig. 12(d) with the exact numerical solution (red line) of the Landau-Lifshitz equations after an evolution time $t = 100$ with the same boundary conditions as in Fig. 12(d): $(v_L, w_L) = (-0.33, 0.91)$, $(v_R, w_R) = (0.91, -0.33)$ which corresponds to $r_-^L = r_-^R = -0.7$, $r_+^L = r_+^R = 0.1$.

w_i the following expressions:

$$w_1 = -\sqrt{\tfrac{1}{2}\big[1 + \big(2\lambda_2^2 - 1\big)S_{1,2}^{(+)} - 2\lambda_2\lambda_2' E_{1,2}^{(-)}\big]}, \quad (111a)$$

$$w_2 = -\sqrt{\tfrac{1}{2}\big[1 + \big(2\lambda_2^2 - 1\big)S_{1,2}^{(+)} + 2\lambda_2\lambda_2' E_{1,2}^{(-)}\big]}, \quad (111b)$$

and at the small amplitude edge (where $\lambda_4 = 1$) the expression

$$w_1 = w_2 = -\sqrt{\tfrac{1}{2}(1 + \lambda_1\lambda_2 + \lambda_1'\lambda_2')}, \quad (112)$$

with the same formula (96c) for w_3 and w_4 at both edges.

If instead we consider the case where $f_1 > 0$ is given Eq. (32b), we obtain the CDSW shown in Fig. 12(b) which corresponds to the opposite transition $B_1 \to A_1$. At the soliton edge (where $\lambda_4 = \lambda_2$) we obtain the expressions

$$w_3 = -\sqrt{\tfrac{1}{2}\big[1 + \big(2\lambda_2^2 - 1\big)S_{1,2}^{(-)} + 2\lambda_2\lambda_2' E_{1,2}^{(+)}\big]}, \quad (113a)$$

$$w_4 = \sqrt{\tfrac{1}{2}\big[1 + \big(2\lambda_2^2 - 1\big)S_{1,2}^{(-)} - 2\lambda_2\lambda_2' E_{1,2}^{(+)}\big]}, \quad (113b)$$

and at the small amplitude edge (where $\lambda_4 = 1$)

$$w_3 = -w_4 = -\sqrt{\tfrac{1}{2}(1 + \lambda_1\lambda_2 - \lambda_1'\lambda_2')}, \quad (114)$$

with the same formula (98a) for w_1 and w_2 at both edges. Considering the other cases, with $f_1 < 0$ leads to CDSWs represented in Figs. 12(c) and 12(d) and corresponding to the transitions $B_2 \to A_2$ and $A_2 \to B_2$ respectively. In Fig. 13 we compare the analytic solution with the exact numerical solution of the Landau-Lifshitz equation for the boundary conditions corresponding to Fig. 12(d). As we see, there is a very good agreement of the envelope functions with the numerical results

In a similar way one can consider solutions schematically depicted in Fig. 11(b). They correspond to transitions $A_1 \leftrightarrow A_2$ or $B_1 \leftrightarrow B_2$ which cross the antidiagonal $w = -v$ of

Fig. 10. If we take $f_1 > 0$ given by Eq. (32a), at the soliton edge ($\lambda_2 = \lambda_3$) we obtain the expressions

$$w_3 = \sqrt{\tfrac{1}{2}\big[1 + \big(2\lambda_3^2 - 1\big)S_{3,4}^{(+)} - 2\lambda_3\lambda_3' E_{3,4}^{(-)}\big]}, \quad (115a)$$

$$w_4 = \sqrt{\tfrac{1}{2}\big[1 + \big(2\lambda_3^2 - 1\big)S_{3,4}^{(+)} - 2\lambda_3\lambda_3' E_{3,4}^{(-)}\big]}, \quad (115b)$$

and at the small amplitude edge ($\lambda_2 = -1$)

$$w_3 = w_4 = \sqrt{\tfrac{1}{2}(1 + \lambda_3\lambda_4 + \lambda_3'\lambda_4')}, \quad (116)$$

with the same formula (100a) for w_1 and w_2 at both edges. If we take $f_1 < 0$, then these expressions merely change sign upon appropriate reordering. At last, for the case $f_1 > 0$ given by Eq. (32b) we obtain at the soliton edge ($\lambda_2 = \lambda_3$) the expressions

$$w_3 = -\sqrt{\tfrac{1}{2}\big[1 + \big(2\lambda_3^2 - 1\big)S_{3,4}^{(-)} - 2\lambda_3\lambda_3' E_{3,4}^{(+)}\big]}, \quad (117a)$$

$$w_4 = \sqrt{\tfrac{1}{2}\big[1 + \big(2\lambda_3^2 - 1\big)S_{3,4}^{(-)} - 2\lambda_3\lambda_3' E_{3,4}^{(+)}\big]}, \quad (117b)$$

and at the small amplitude edge ($\lambda_2 = -1$)

$$w_3 = -w_4 = -\sqrt{\tfrac{1}{2}(1 + \lambda_3\lambda_4 - \lambda_3'\lambda_4')}, \quad (118)$$

with the same formula (102a) for w_1 and w_2 at both edges. Again, if we take $f_1 < 0$, then these expressions will also change signs upon appropriate reordering.

We now turn to the study of the generalizations of CDSWs by considering the transitions depicted in Fig. 14: in these cases the boundary points are also not in the same monotonicity triangle of the (v, w) plane; still on the same ellipse because the left and right boundary conditions have a common value for one of the Riemann invariants (say, $r_-^L = r_-^R$), however the boundary values of the other Riemann invariants are different ($r_+^L \neq r_+^R$). To be definite, we shall
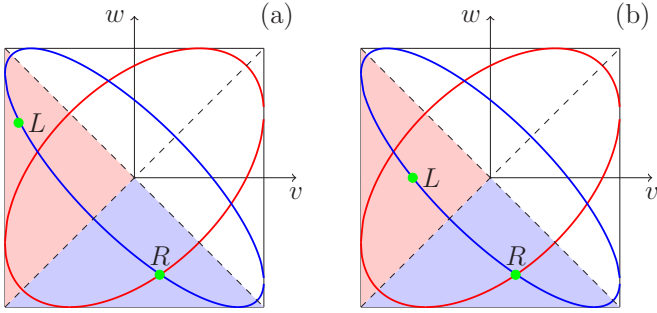
FIG. 14. Paths in the (v,w) plane associated with two types of combined shocks. The left and right boundary conditions correspond to points L and R respectively; they lie on an ellipse along which the dispersionless Riemann invariant r_- ($= r_-^L = r_-^R$) is constant. One has $r_+^L < r_+^R$ in case (a) and $r_+^L > r_+^R$ in case (b).

consider two generalizations of the situation leading to the CDSW represented in Figs. 12(d) and 13. The transition of the type $A_2 \rightarrow B_2$ of Fig. 10 can be generalized in two ways represented in Fig. 14, where the points L and R symbolize plateaus at the left and right boundaries, respectively. In this case $r_-^L = r_-^R$ because the transition occurs along the ellipse where this Riemann invariant is constant. As we know, the dispersionless invariant r_+ decreases along such a curve when going away from the diagonal $w = v$, hence we have $r_+^L < r_+^R$ and $r_+^L > r_+^R$ in case (a) and (b), respectively. This suggests the generalizations of the diagram Fig. 11(a) depicted in Fig. 15.

In the case corresponding to Fig. 15(a), the CDSW is attached at its soliton edge to a rarefaction wave which matches at its left edge with the left boundary plateau. The velocities of the characteristic points identified in Fig. 15(a) are expressed in terms of the boundary Riemann invariants by the formulas

$$s_-^{(1)} = \frac{1}{2}(r_-^L + 3r_+^L), \quad s_-^{(2)} = \frac{1}{2}(3r_+^R + r_-^R),$$
$$s_+ = 2 + \frac{(r_+^R - r_-^R)^2}{2(r_+^R + r_-^R - 2)}. \tag{119}$$

The resulting composite wave structure is shown in Fig. 16 (blue line) where it is compared with the numerical solution of the Landau-Lifshitz equation (red line).

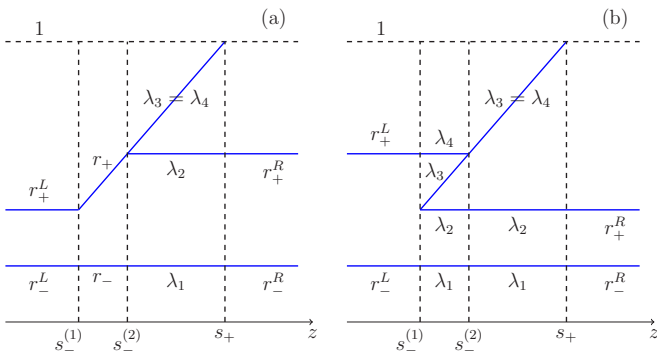In the case corresponding to Fig. 15(b) the trigonometric CDSW is attached to a cnoidal DSW of the type Fig. 8(a)

FIG. 15. Sketches of the behavior of the Riemann invariants corresponding to the transitions in the (v,w) plane shown in Fig. 14.
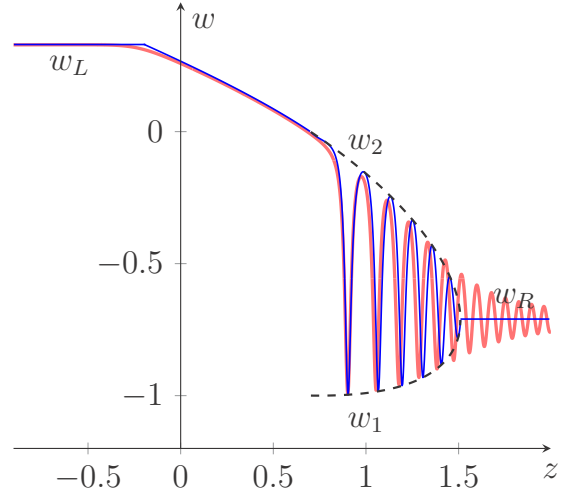

FIG. 16. Comparison of the analytic solution corresponding to the left and right boundary conditions depicted in Fig. 15(a) with the exact numerical solution of the Landau-Lifshitz equations.

which degenerates at its right edge (at which $w_2 = w_1$) into a trigonometric wave. At the left soliton edge the cnoidal wave matches with the left boundary plateau. The velocities of the characteristic points identified in Fig. 15(b) are given by

$$s_-^{(1)} = \frac{1}{2}(r_-^L + 2r_+^R + r_+^L),$$
$$s_-^{(2)} = 2r_+^L + \frac{(r_+^R - r_-^R)^2}{2(r_+^R + r_-^R - 2r_+^L)}, \tag{120}$$
$$s_+ = 2 + \frac{(r_+^R - r_-^R)^2}{2(r_+^R + r_-^R - 2)}.$$

The resulting composite wave structure is shown in Fig. 17 (blue line) where it is compared with the numerical solution of the Landau-Lifshitz equation (red line).

It is clear that any transition between points shown in Fig. 10 can be generalized in a similar way leading to composite shock
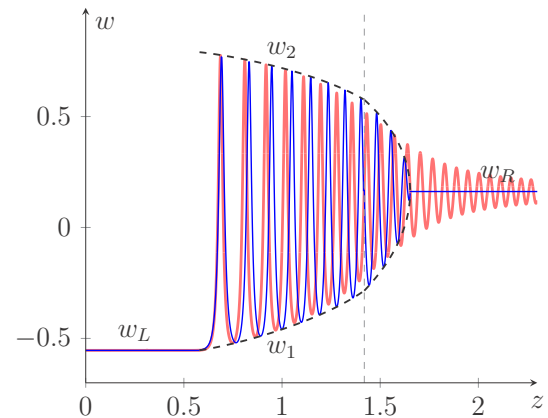

FIG. 17. Comparison of the analytic solution corresponding to the left and right boundary conditions depicted in Fig. 15(b) with the exact numerical solution of the Landau-Lifshitz equations. The (analytically determined) vertical dashed line separates the cnoidal wave (at the left) from the trigonometric wave (at the right).
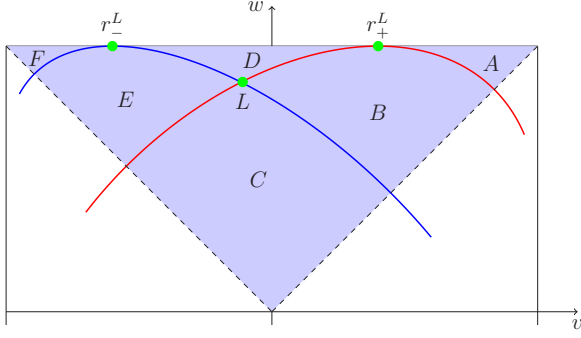
FIG. 18. Plot of the upper monotonicity triangle of NLS type in the (v,w) plane. The (red and blue) curves of constant dispersionless Riemann invariants $r_\pm^L$ corresponding to the left boundary point L divide this triangle into six domains denoted as A, B, ..., F. The type of flow depends on the domain in which lies the right boundary point R of coordinates (v_R, w_R).

waves consisting of cnoidal, trigonometric, and rarefaction waves. We shall not list here all these possible wave structures since the general principles for their construction are simply deduced from the examples just presented.

This ends the characterization of all the key elements which may appear in a complex wave structure evolving from an arbitrary initial discontinuity of type (72). We can now proceed to the classification of all the possible composite structures.

V. CLASSIFICATION

As clear from the previous section, it is convenient to distinguish the situations where both points representing the left and right boundary conditions belong to the same triangle of monotonicity from those where they belong to different such triangles. It has been noticed in Sec. II 1 that in these triangles, for some limiting values of the variables, the Landau-Lifshitz equation reduces either to the NLS or to KB equation. We shall thus refer to such triangles as being of "NLS type" or of "KB type," and consider them separately.

A. Nonlinear Schrödinger type sector

Since the theory for the upper and lower NLS type triangles is essentially the same, we shall confine ourselves to the upper triangle which is shown in Fig. 18.

We thus consider the case where both left and right initial conditions correspond to points located inside this triangle of the (v,w) plane. For definiteness, we denote the point of coordinates (v_L, w_L) referring to the left boundary by L and plot the two ellipses of constant Riemann invariants r_+^L and r_-^L. These divide the triangle into six subdomains. It is easy to see that, when the point R referring to the right boundary is located in one of these domains (labeled by the symbols A, B,..., F), one of the following inequalities is fulfilled:

(A) $\quad r_-^L < r_+^L < r_-^R < r_+^R,$ (B) $\quad r_-^L < r_-^R < r_+^L < r_+^R,$

(C) $\quad r_-^R < r_-^L < r_+^L < r_+^R,$ (D) $\quad r_-^L < r_-^R < r_+^R < r_+^L,$

(E) $\quad r_-^R < r_-^L < r_+^R < r_+^L,$ (F) $\quad r_-^R < r_+^R < r_-^L < r_+^L.$
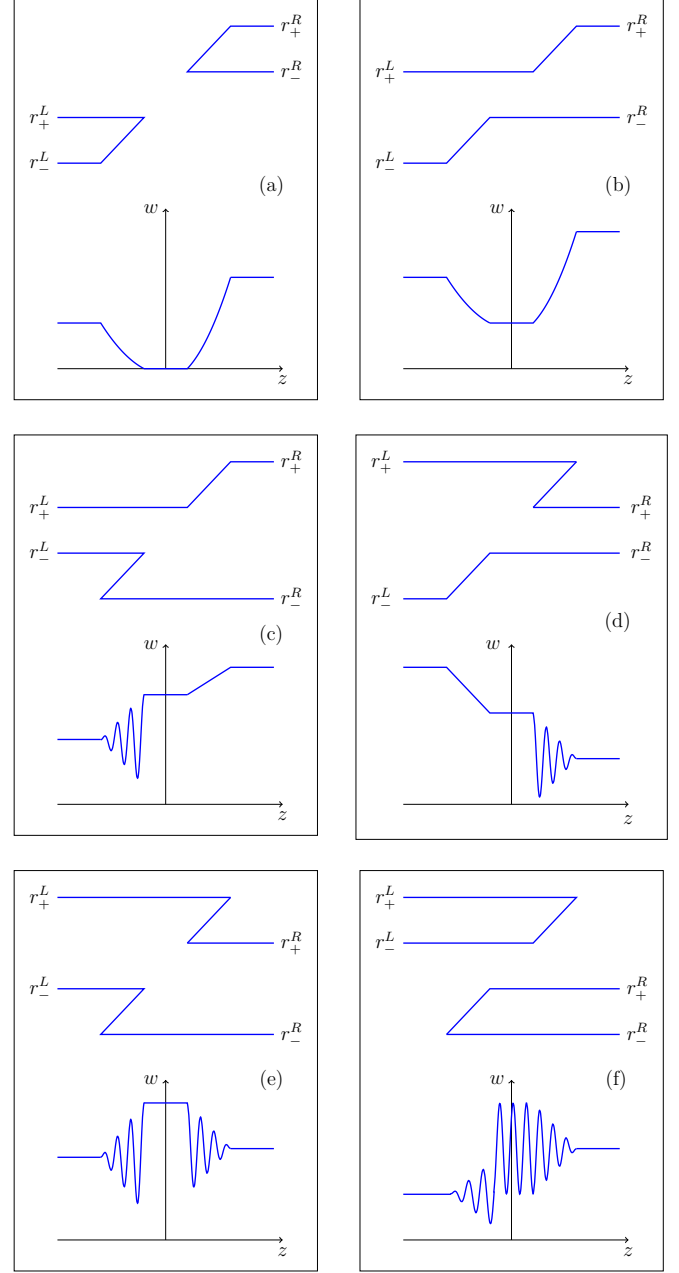
$$(121)$$

FIG. 19. Sketches of the behavior of the Riemann invariants and of the corresponding wave structures corresponding to the location of the point R referring to the right boundary in one of the six domains shown in Fig. 18.

The corresponding diagrams of the Riemann invariants symbolizing the self-similar solutions of the Whitham equations and sketches of wave structures are shown in Fig. 19. In case (A) the structure consists of two rarefaction waves expanding into "vacuum" and in case (B) these two rarefaction waves are connected by a plateau whose parameters are determined by the dispersionless Riemann invariants $r_\pm^P$ equal to $r_-^P = r_-^R$ and $r_+^P = r_+^L$. In cases (C) and (D) the structure consists of one DSW and one rarefaction wave connected by a plateau characterized by the same parameters. In case (E) there are two DSWs connected by a plateau and, at last, in case (F) the

previous plateau is replaced by a nonlinear wave which—with high enough accuracy—can be presented as a nonmodulated cnoidal wave. Not surprisingly, this classification coincides qualitatively with the one obtained in Ref. [23] for the NLS equation. It is clear that it is determined by the geometry of the curves of constant Riemann invariants: the arcs of ellipses shown in Fig. 18 become, in the NLS equation, arcs of parabolas with the same subdivision of the monotonicity region which, in the NLS case, extends to the whole half plane of all possible values of the physical parameters. In the present Landau-Lifshitz case, a typical example of such a structure has been studied in some details in Ref. [13].

It is important to notice that the domains A and F cannot be reached from point L in Fig. 18 via paths consisting of arcs of constant dispersionless Riemann invariants without bypassing the points labeled as r_-^L and r_+^L, at which the meaning of the Riemann invariants changes (see Fig. 2 and the related discussion in the text). Therefore, in these two cases, the edge wave structures are separated either by vacuum (i.e., $w = 0$) in case (A), or by a cnoidal wave in case (F). In the other situations (B, C, D, E) we can draw two arcs of constant invariant ellipses whose crossing point defines the plateau connecting the edge wave structures (rarefaction waves or DSWs). It is easy to see that these two arcs can be drawn in two ways and that the physically relevant one is distinguished by the condition that the speeds of the matching points increase from left to right (see a similar argumentation in the theory of standard viscous shock waves in Ref. [17]). Consequently, the left edge wave always corresponds to a diagram of Riemann invariants with $r_+^L = $ const continued through the whole left wave, whereas in the right edge wave we have $r_-^R = $ const also continued through the whole right structure. Diagrams (B)–(E) in Fig. 19 illustrate this simple principle. This remark removes any ambiguity in the determination of the wave structure arising from initial conditions referring to the NLS type sectors.

B. Kaup-Boussinesq type sector

We shall now consider initial conditions for which both left and right boundary points are located in a KB sector of the (v, w) plane which consists of one of the triangles delimited by the diagonal, the antidiagonal, and the vertical curve $v = \pm 1$. For definiteness we consider the right KB triangle. This situation bares many similarities with the preceding NLS type case. Indeed, from Fig. 20 we see that, again, the monotonicity triangle is divided into six domains corresponding to the inequalities listed in Eq. (121)—these domains are symmetrical with respect to the diagonal $w = v$ to those shown in Fig. 18. It is clear that the diagrams of Riemann invariants and the corresponding wave structures are qualitatively the same as the ones depicted in Fig. 19. A detailed discussion of the Riemann problem for the KB equation (15) has been recently given in Ref. [25] and in the KB sector of Landau-Lifshitz equation theory the resulting wave patterns are qualitatively the same—they consist of DSWs and/or rarefaction waves connected with each other by plateaus.

As in the NLS type sectors, if the point R referring to the right boundary lies in one of the domains B, C, D, or E, it can be connected with L by two arcs of constant Riemann invariant
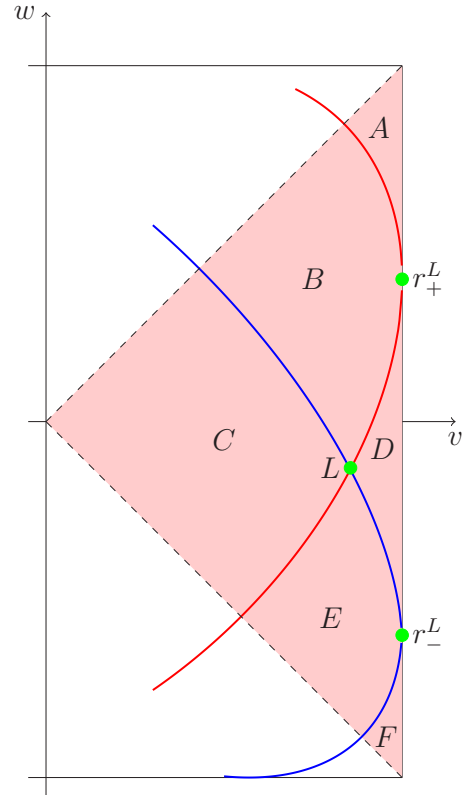

FIG. 20. Plot of the right monotonicity triangle of KB type in the (v, w) plane. The (red and blue) curves of constant dispersionless Riemann invariants $r_\pm^L$ corresponding to the left boundary point L divide this triangle into six domains denoted as A, B, ..., F. The type of flow depends on the domain in which lies the right boundary point R of coordinates (v_R, w_R).

ellipses in two possible ways; the physically acceptable one is identified by the condition that the speeds of the matching points increase from left to right. The crossing point of these two arcs defines the parameter of the plateau which connects the two edge wave structures. In cases (A) and (F) the plateau does not exist and is replaced either by a vacuum region or by a nonmodulated cnoidal wave. We thus arrive at the same wave structures that the ones illustrated in Fig. 19.

C. Wave structures with transitions between monotonicity sectors

The above formulated principles of construction of diagrams for the Riemann invariants make it possible to predict which wave structure will evolve from a given boundary condition (72), even in cases where the left and right boundary points belong to different triangles of monotonicity. Since the total number of possible wave structures is very large, we shall not list all of them here but rather illustrate the principles of construction by an application to a typical particular case.

Let us take $v_L = v_R = 0$, $w_L < 0$, $w_R > 0$, and $|w_L| < w_R$. We see at once from Fig. 21(a) that the dispersionless ellipses relating L to R must cross both diagonals of the hyperbolicity square, hence the wave structure must consist of two contact and/or combined waves. Substitution of the above parameters into Eq. (75) yields the values of the dispersionless Riemann
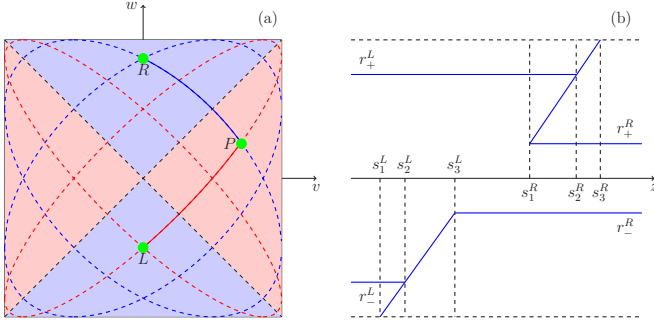
FIG. 21. (a) Plot in the (v,w) plane of ellipses along which the dispersionless Riemann invariants are constant. They are represented by red (blue) dashed lines for the left (right) boundary conditions. The path connecting the left L and the right R points are shown by solid lines. They intersect at point P representing the plateau located between the left and right waves. (b) Sketch of the behavior of the Riemann invariants corresponding to solutions of the Whitham equations for the same boundary conditions. The left wave consists of a trigonometric shock (for $s_1^L < z < s_2^L$) attached to a rarefaction wave (for $s_2^L < z < s_3^L$). The right wave is a combined cnoidal ($s_1^R < z < s_2^R$) and trigonometric ($s_2^R < z < s_3^R$) shock.
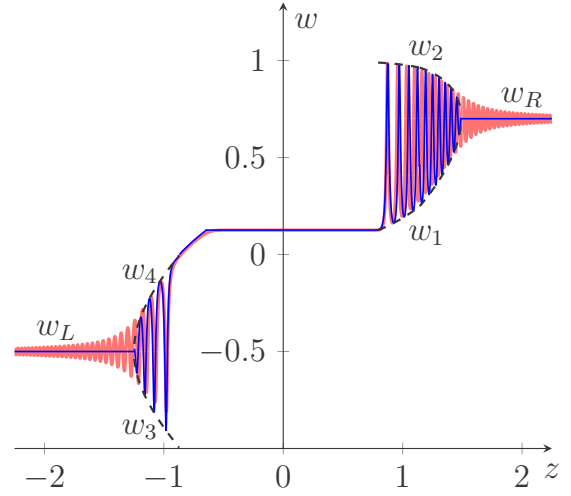

FIG. 22. Comparison of analytic (blue line) and numerical (red line) solutions for the initial profile (72) with $v_L = v_R = 0$, $w_L = -0.5$, $w_R = 0.7$. The left and right boundary points are represented in Fig. 21(a) and the behavior of the Riemann invariants is sketched in Fig. 21(b).

invariants which are ordered according to $r_-^L < r_-^R < r_+^R < r_+^L$. Taking into account that the left wave corresponds to the continuation of $r_+^L = $ const and the right wave to the continuation of $r_-^R = $ const, we arrive at the diagram shown in Fig. 21(b). At the left edge we have the combination of a trigonometric shock ($s_1^L \leqslant z \leqslant s_2^L$) with a rarefaction wave ($s_2^L \leqslant z \leqslant s_3^L$) and, at the right edge, one has merged cnoidal ($s_1^R \leqslant z \leqslant s_2^R$) and trigonometric ($s_2^R \leqslant z \leqslant s_3^R$) shocks. These left and right edge waves are connected one with the other by a plateau characterized by the Riemann invariants $r_-^P = r_-^R$ and $r_+^P = r_+^L$. This plateau is represented by the single point P in Fig. 21(a).

The formulas connecting the zeros w_i of the resolvent with the Riemann invariants λ_i (obtained as solutions of the Whitham equations) are of the type discussed in Sec. IV C. They make it possible to explicitly construct the Whitham wave structure (shown in Fig. 22 by a blue line) which compares very well with the numerical solution of the Landau-Lifshitz equation (red line). This example clearly illustrates how the wave structure can be constructed for any choice of parameters of the initial discontinuous profile (72).

VI. DISCUSSION AND CONCLUSION

In this paper we have solved the Riemann problem and characterized the space-time evolution of an initial discontinuity for the Landau-Lifshitz equation. This equation describes magnetization excitations in a dissipationless easy-plane ferromagnet and, in the appropriate regime corresponding to the conditions (2), polarization waves in a two-component BEC. It is natural to suppose that the method developed in the present work is general enough and should apply to many other models. We shall thus formulate the most important points of our approach.

(i) The first obvious feature is the statement that the method in its present form applies to modulationally stable situations only, so the region of hyperbolicity of the long wave

(dispersionless) approximation should be determined and the boundary conditions at both sides of the discontinuity must lie within this region.

(ii) The hyperbolicity region should be subdivided into domains where the dispersionless approximation is *genuinely nonlinear* (see, e.g., Ref. [30]), i.e., where the characteristic velocities depend on the field variables with nonvanishing gradients. In our case—with two field variables with known Riemann invariants—we have denoted such domains as *monotonicity sectors*. For systems described by a single field variable, this condition reduces to imposing a fixed convexity to the dependence of the dispersionless velocity on the amplitude of the wave; an example of such a situation was considered in Ref. [27].

(iii) If both boundary conditions belong to the same monotonicity sector, then the classification of the wave structures follows closely well-known examples such as KdV (one field variable [18]) or NLS (two field variables [23]) theories. These wave structures consist of rarefaction waves and standard dispersive shock waves of Gurevich-Pitaevskii type connected with each other by a plateau, a "vacuum" or a two-phase (i.e., nonmodulated "cnoidal") wave region.

(iv) If the boundary conditions belong to different monotonicity sectors, then they are connected by profiles consisting of new wave structures—contact (trigonometric) dispersive shocks or kinks. In situations with a single field variables these were identified, respectively, in Refs. [26] and [29]; both structures appeared also in the theory of the Gardner equation [27]. In the case considered here of the Landau-Lifshitz equation we have dealt with contact dispersive shock waves and their combinations with other structures.

(v) When the evolution equations are completely integrable, the Whitham system can be transformed into a diagonal Riemann form and in this case the mapping of the Riemann invariants to the physical parameters is not single valued. Instead, it is realized by sets of relationships between the

zeros of two polynomials: the polynomial whose roots are the Riemann invariants (noted P in the main text) and its algebraic resolvent ($\mathcal{R}$). These relationships appear in a natural way in the finite-gap integration method (see, e.g., Ref. [54]) complemented by resolving the problem of "reality conditions" [48] (see also Ref. [51]). For the Landau-Lifshitz equation the corresponding resolvent was found in Ref. [44] in which, however, the consequences of the multiplicity of relationships between the Riemann invariants and the zeros of the resolvent were not completely elucidated. The theory developed in the present work clarifies this important point.

We thus believe that the solution of the Riemann problem for the case of nonlinear waves whose evolution is governed by the Landau-Lifshitz equations provides a general scheme which applies to other systems which share the similar characteristic property of not being genuinely nonlinear, cf. the case of the modified NLS equation considered in Ref. [55]. Besides, the different situations considered in the present work can find applications for describing nonlinear waves in concrete physical situations such as ferromagnets and two-component Bose-Einstein condensates.

[1] M. H. Anderson, J. R. Ensher, M. R. Matthews, C. E. Wieman, and E. A. Cornell, Science **269**, 198 (1995).

[2] K. B. Davis, M.-O. Mewes, M. R. Andrews, N. J. van Druten, D. S. Durfee, D. M. Kurn, and W. Ketterle, Phys. Rev. Lett. **75**, 3969 (1995).

[3] C. J. Myatt, E. A. Burt, R. W. Ghrist, E. A. Cornell, and C. E. Wieman, Phys. Rev. Lett. **78**, 586 (1997).

[4] J. Stenger, S. Inouye, D. M. Stamper-Kurn, H.-J. Miesner, A. P. Chikkatur, and W. Ketterle, Nature (London) **396**, 345 (1998).

[5] D. S. Hall, M. R. Matthews, J. R. Ensher, C. E. Wieman, and E. A. Cornell, Phys. Rev. Lett. **81**, 1539 (1998).

[6] Y. Kawaguchi and M. Ueda, Phys. Rep. **520**, 253 (2012).

[7] D. M. Stamper-Kurn and M. Ueda, Rev. Mod. Phys. **85**, 1191 (2013).

[8] C. J. Pethick and H. Smith, *Bose-Einstein Condensation in Dilute Gases* (Cambridge University Press, Cambridge, England, 2002).

[9] L. Pitaevskii and S. Stringari, *Bose-Einstein Condensation* (Clarendon, Oxford, 2003).

[10] *Emergent Nonlinear Phenomena in Bose-Einstein Condensates: Theory and Experiment*, edited by P. G. Kevrekidis, D. J. Frantzeskakis, and R. Carretero-González (Springer, Berlin, 2007).

[11] A. M. Kamchatnov, Y. V. Kartashov, P.-É. Larré, and N. Pavloff, Phys. Rev. A **89**, 033618 (2014).

[12] C. Qu, L. P. Pitaevskii, and S. Stringari, Phys. Rev. Lett. **116**, 160402 (2016).

[13] T. Congy, A. M. Kamchatnov, and N. Pavloff, SciPost Phys. **1**, 006 (2016).

[14] T. Bienaimé, E. Fava, G. Colzi, C. Mordini, S. Serafini, C. Qu, S. Stringari, G. Lamporesi, and G. Ferrari, Phys. Rev. A **94**, 063652 (2016).

[15] C. Hamner, J. J. Chang, P. Engels, and M. A. Hoefer, Phys. Rev. Lett. **106**, 065302 (2011).

[16] I. Danaila, M. A. Khamehchi, V. Gokhroo, P. Engels, and P. G. Kevrekidis, Phys. Rev. A **94**, 053617 (2016).

[17] L. D. Landau and E. M. Lifshitz, *Fluid Mechanics* (Pergamon, Oxford, 1959).

[18] A. V. Gurevich and L. P. Pitaevskii, Zh. Eksp. Teor. Fiz. **65**, 590 (1973) [Sov. Phys. JETP **38**, 291 (1974)].

[19] G. B. Whitham, Proc. R. Soc. London **283**, 238 (1965).

[20] G. B. Whitham, *Linear and Nonlinear Waves* (Wiley Interscience, New York, 1974).

[21] G. A. El and M. A. Hoefer, Physica D **333**, 11 (2016).

[22] A. V. Gurevich and A. L. Krylov, Zh. Eksp. Teor. Fiz. **92**, 1684 (1987) [Sov. Phys. JETP **65**, 944 (1987)].

[23] G. A. El, V. V. Geogjaev, A. V. Gurevich, and A. L. Krylov, Physica D **87**, 186 (1995).

[24] G. A. El, R. H. J. Grimshaw, and M. V. Pavlov, Stud. Appl. Math. **106**, 157 (2001).

[25] T. Congy, S. K. Ivanov, A. M. Kamchatnov, and N. Pavloff, Chaos **27**, 083107 (2017).

[26] T. R. Marchant, Wave Motion **45**, 540 (2008).

[27] A. M. Kamchatnov, Y.-H. Kuo, T.-C. Lin, T.-L. Horng, S.-C. Gou, R. Clift, G. A. El, and R. H. J. Grimshaw, Phys. Rev. E **86**, 036605 (2012).

[28] G. A. El, M. A. Hoefer, and M. Shearer, SIAM Rev. **59**, 3 (2017).

[29] J. G. Esler and J. D. Pearce, J. Fluid Mech. **667**, 555 (2011).

[30] P. D. Lax, *Hyperbolic Partial Differential Equations*, Courant Lecture Notes, Vol. 14 (AMS, New-York, 2006).

[31] L. D. Landau and E. M. Lifshitz, Phys. Z. Sowjet. **8**, 153 (1935).

[32] E. M. Lifshitz and L. P. Pitaevskii, *Statistical Physics, Part II* (Nauka, Moscow, 1978).

[33] H. Lacombe, La Houille Blanche **1**, 38 (1965).

[34] L. V. Ovsyannikov, J. Appl. Mech. Tech. Phys. **30**, 127 (1979) [Zh. Prikl. Mekh. Tekch. Fiz. **2**, 3 (1979)].

[35] A. G. Cavanié, Cah. Oceanogr. **29**, 831 (1969).

[36] H. Sandstrom and C. Quon, Fluid Dyn. Res. **11**, 119 (1993).

[37] V. Yu. Liapidevskii and V. M. Teshukov, *Mathematical Models of Long Wave Propagation in an Inhomogeneous Fluid*, Izd. Sib. Otd. Ross. Akad. Nauk [in Russian] (Novosibirsk, 2000).

[38] A. M. Kosevich, B. A. Ivanov, and A. S. Kovalev, Phys. Rep. **194**, 117 (1990).

[39] E. Iacocca and M. A. Hoefer, Phys. Rev. B **95**, 134409 (2017).

[40] E. Iacocca, T. J. Silva, and M. A. Hoefer, Phys. Rev. Lett. **118**, 017203 (2017).

[41] D. T. Son and M. A. Stephanov, Phys. Rev. A **65**, 063621 (2002).

[42] A. E. Borovik, Pis'ma Zh. Eksp. Teor. Fiz. **28**, 629 (1978) [JETP Lett. **28**, 629 (1978)].

[43] A. E. Borovik, S. Klama, and S. I. Kulinich, Physica D **32**, 107 (1988).

[44] A. M. Kamchatnov, Zh. Eksp. Teor. Fiz. **102**, 868 (1992) [JETP **75**, 1606 (1992)].

[45] C. K. Law, C. M. Chan, P. T. Leung, and M.-C. Chu, Phys. Rev. A **63**, 063612 (2001).

[46] D. J. Kaup, Prog. Theor. Phys. **54**, 396 (1975).

[47] G. A. El, Chaos **15**, 037103 (2005).

[48] A. M. Kamchatnov, J. Phys. A: Math. Gen. **23**, 2945 (1990).

[49] M. Abramowitz and I. A. Stegun, *Handbook of Mathematical Functions* (Dover, New York, 1972).

[50] A. M. Kamchatnov, Phys. Lett. A **186**, 387 (1994).

[51] A. M. Kamchatnov, *Nonlinear Periodic Waves and Their Modulations—An Introductory Course* (World Scientific, Singapore, 2000).

[52] R. Courant and K. O. Friedrichs, *Supersonic Flow and Shock Waves* (Interscience, New York, 1956).

[53] S. K. Ivanov and A. M. Kamchatnov, Zh. Eksp. Teor. Fiz. **151**, 644 (2017) [JETP **124**, 546 (2017)].

[54] V. E. Zakharov, S. V. Manakov, S. P. Novikov, and L. P. Pitaevskii, *The Theory of Solitons: The Inverse Scattering Method* (Nauka, Moscow, 1980) (translation: Consultants Bureau, 1984).

[55] S. K. Ivanov and A. M. Kamchatnov, Phys. Rev. A **96**, 053844 (2017).